IONOSPHERIC NEUTRAL WIND AND ELECTRIC FIELD MEASUREMENTS USING BARIUM AND STRONTIUM CLOUDS

by

R.A. Mountford, B.Sc.

A thesis submitted to the
University of Southampton
for the degree of
Master of Philosophy

July 1975

ABSTRACT

FACULTY OF SCIENCE

PHYSICS

Master of Philosophy

IONOSPHERIC NEUTRAL WIND AND ELECTRIC FIELD MEASUREMENTS USING BARIUM AND STRONTIUM CLOUDS

by Rosemary Anne Mountford

Barium ion and strontium neutral clouds, released at auroral and sub-auroral latitudes, have been used to investigate ionospheric neutral winds. The observations made on these clouds at magnetically quiet times are in good agreement with theoretical predictions. During magnetic disturbance, evening releases provide information which can be interpreted equally as supporting ion drag or auroral heating as the dominant mechanism modifying the quiet time wind system. Results of morning releases, however, suggest that auroral heating is the dominant mechanism.

A barium cloud which was released at 129 km and did not separate into neutral and ionised components has been analysed using an alternative theory of ion cloud motion, instead of the theory devised by Haerendel which is usually used in calculating electric field values from barium cloud experiments. The results obtained by applying this alternative theory to a cloud which did not separate, but may have contained ions, suggest that this theory may be of value in circumstances where the Haerendel theory cannot be used.

ACKNOWLEDGEMENTS

I am extremely grateful to my supervisor, Miss P.Rothwell, for her constant guidance and encouragement throughout this project. It was run jointly with the Physics Department of the University of Sussex and my sincere thanks go to Dr. G.Martelli who directed the project in Sussex, and to fellow research students Dr. J.Hunter, Dr. M.Giles and Mrs. H.Hilmi, all of Sussex University.

Generous assistance has been provided by Miss W.Tomsett in obtaining and analysing data, and Mr. D.Fryer, the chief photographer for this project.

I have benefited from discussions with Dr. J.W.King of the Appleton Laboratory, Slough and Dr. R.Rüster of the Max Planck Institut für Aeronomie, W.Germany. Also, Dr. King generously provided the computed quiet time neutral wind values used in part of the analysis.

I am indebted to the professors of physics in the University of Southampton, in particular Professor G.W.Hutchinson, for making laboratory facilities available to me, and to the University of Southampton for the provision of a grant.

CONTENTS

Chapter One

INTRODUCTION

1.1 Chemical release experiments

In recent years extensive use has been made of chemical release experiments in studying the upper atmosphere. Initially, such experiments could only be used to study ionospheric neutral winds, since the clouds consisted entirely of neutral particles (Rosenberg et al. 1964, Groves 1960, Murphy et al. 1966). Subsequently, the technique has been brought into wider use with the introduction of a means of producing clouds of ions. Using ion clouds, experiments have been performed in an attempt to establish a pattern for ionospheric electric fields. More recently, interest has again centered on neutral wind studies, because of the possibility of interaction between ions, moving under the influence of the electric field, and the neutral wind.

The chemicals normally used in these experiments are

i) barium, which produces ionised vapour clouds for electric field studies

ii) stontium, which produces electrically neutral vapour clouds for neutral wind studies.

The vapour is released from a sounding rocket or a satellite at an appropriate height, and information is obtained by photographing the motion and development of the cloud, or clouds, from the ground.

The earliest chemical release experiments, performed in the late 1950s and early 1960s, used sodium vapour for neutral wind studies. The chemical was released steadily from an ascending rocket to form a 'trail' of vapour

extending over an altitude range of several tens of kilometres (Manring et al. 1959, Manring et al. 1964, Kochanski 1964). The sodium vapour was visible at twilight because of resonance scattering of solar radiation by the D lines. The trails were photographed from three observation sites, and an analog method was used to determine from these photographs the locus of the trail in space.

Subsequently, trimethyl-aluminium (TMA) was used to produce vapour trails similar to the sodium trails, but with the advantage that TMA is visible both in twilight (by resonance scattering of solar radiation) and in darkness (by chemiluminescent emission because of interaction with atmospheric oxygen atoms). Thus neutral wind observations could be made during the night as well as at dusk and dawn (Stoffregen 1971).

In 1963 experiments were performed to test various percentages of barium and strontium in combination with other chemicals, in an attempt to find a way of producing ionised vapour clouds (Haser 1967). It was found that, while about 40% of strontium evaporated compared with 6% of barium, strontium produced no ions at all and barium showed a good ionisation efficiency. A mixture of copper oxide and barium, containing excess barium was found to give the best evaporation efficiency, in the reaction

$$(n+1)Ba + CuO = BaO + Cu + nBa$$

as reported by Föppl et al. (1967). Ba chemical release payloads therefore consist of a pressurised mixture of CuO and Ba granules, with a timing device and igniters to initiate the reaction. The Ba metal used in payloads always contains a small amount of Sr as an impurity, and

consequently both an ionised Ba and a neutral Sr cloud are produced at the same time. When neutral clouds only are required, Sr granules replace the Ba in the payload.

The clouds can be seen from the ground because both Ba and Sr have resonance lines in the visible spectrum. Therefore if the clouds are against a reasonably dark sky background but are themselves in sunlight, they are readily visible. Moreover, Ba clouds must be in sunlight because it is solar ultra-violet radiation which is responsible for production of the Ba ions. It is thus necessary for these experiments to be performed during twilight.

The data obtained from experiments of this type is in the form of photographic records, obtained simultaneously from two or more ground observation sites. The sites are chosen to provide a long enough base line for triangulation, in order to determine cloud positions by reference to the fixed star background.

1.2 Ionospheric electric fields

Ionospheric electric fields are of interest because they give information on the convective interaction between the magnetosphere and the solar wind (Taylor and Hones 1965, Axford and Hines 1961). A comparison of electric fields in magnetically quiet and disturbed conditions is of particular value because effects such as aurora, which occur or are enhanced during magnetic disturbance, are thought to result from this interaction.

The electric fields, although measured in the ionosphere, can give information concerning the outer regions of the magnetosphere, because the magnetic field is 'frozen in' the plasma. That is to say, there is direct association of

a particular flux tube in the magnetosphere and the ionisation which it contains. Thus convective motions which occur in a particular part of the magnetosphere can be expected to produce electric fields in that part of the ionosphere to which it is linked by the 'frozen in' field, and so measurements of the magnitude and direction of the electric field will give information on the convective motion which produced it.

Initially, ionospheric electric fields were measured in 'probe' experiments. In this method the electric field is calculated from the potential difference between two electrodes extended from a rocket or satellite into the surrounding plasma. After some initial problems in finding a suitable electrode configuration, the method was used successfully in 1966 (Mozer and Bruston, 1967). Since that date many such experiments have been performed and the technique has been further refined (Aggson 1969, Storey 1968, Maynard and Heppner 1970, Maynard and Johnstone 1974).

In the year following Mozer and Bruston's experiment, the ion cloud technique had developed to the stage of being used as an alternative method for measuring electric fields (Haerendel et al. 1969, Wescott et al. 1969, Hunter 1970).

Both experimental techniques have certain advantages and disadvantages. Probe experiments can be used to measure a.c. as well as d.c. fields, and the payloads which carry probe experiments can also carry other equipment to measure relevant ionospheric parameters such as electron temperature and electron number density. However, the time for which data is collected is very short, being only a few hundred seconds. Furthermore, since payloads are complicated and

data is obtained by telemetry transmission, there are many possible areas of failure. This can result in a reduced amount of information being obtained, or in 'noise' which is difficult to distinguish from data.

Ion cloud experiments have the advantage that the payload is very simple and requires no telemetry. Also, the length of time for which data is collected is normally at least ten minutes and can be as much as two hours. However, opportunities for launching ion cloud experiments are limited, both by the twilight requirement and by the necessity for clear skies to allow observation. Moreover the payloads, although simple, need very careful handling since they are effectively explosive. Another disadvantage of the ion cloud method is that the theory on which the interpretation of results is usually based is only truly applicable to altitudes above 150km. (Haerendel et al. 1967). Therefore most experiments have been carried out at around 200km., lower altitudes being almost entirely neglected. A recent advance in the experimental technique is the ejection of ion cloud apparatus from instrumented payloads. The ion cloud is released shortly after being ejected, and the instruments in the remaining payload send back relevant information on ionospheric parameters to help in the interpretation of the ion cloud results.

1.3 Ionospheric neutral winds

The ionosphere is known to behave in a varying fashion, some variations being systematic and time related and others being anomalous and related to location or ambient conditions. To explain some of the anomalous behaviour of the ionosphere, the movement of the neutral atmosphere has

been considered, and models for a global neutral wind system have been set up (Hines 1965, Geisler 1966). In particular, a theoretical neutral wind model for altitudes above 120 km. has been proposed by Kohl and King (1967), using Jacchia's (1965) exospheric temperature distribution.

The model can be tested indirectly, by comparison of experimentally measured values of an ionospheric parameter with theoretical predictions from the model concerning the same parameter. Alternatively it can be tested directly by observing the neutral wind at various times and places by means of chemical releases.

The behaviourof the neutral atmosphere in magnetically quiet conditions is influenced by many forces (e.g. pressure gradient, Coriolis force, viscous force, inertial force) and is already a very complex problem. During magnetic disturbance the situation becomes even more complex, additional forces (e.g. enhanced ion drag, enhanced pressure gradients) are brought into play, and therefore the neutral wind model is no longer applicable. However, in these circumstances the movement of the neutral atmosphere can still be observed using chemical releases and so the influence of the additional forces on the quiet time wind system can be studied.

Chemical release experiments are therefore valuable in the study of neutral winds during both magnetically quiet and disturbed periods.

Neutral winds can be studied using exclusively neutral chemical releases such as TMA, or by using the strontium vapour cloud which always accompanies a barium ion cloud

release. The latter method has the advantage that simultaneous measurements of the neutral wind and the electric field are obtained and so interrelation of these two parameters can be considered. However, TMA has the advantages that it can be used both in twilight and in darkness, and that a trail of the chemical can be released over an altitude range of several tens of kilometres. Thus neutral wind measurements covering a wider range of heights and times can be made using TMA than is possible using strontium vapour clouds.

1.4 Aims of research program

The research program, of which the work to be presented in this thesis forms a part, incorporates both electric field and neutral wind studies at auroral and sub-auroral latitudes. The chemical release experiments to be reported have been launched from ESRANGE, Kiruna, Northern Sweden, and from South Uist, Outer Hebrides, Northern Scotland.

A considerable amount of work has been done by other groups in measuring ionospheric electric fields using ion clouds. The electric field pattern which causes the motion of these clouds, and its relation to magnetic disturbance, is now fairly well established and has been reported by Heppner (1972). However, the theory which is normally applied to ion cloud motion in order to derive electric field values, is valid only above 150km. A further requirement of this theory is that there must be an ion cloud (i.e. it must separate from the neutral cloud) so that its motion can be observed.

An alternative theory which could be applied to ion clouds has been developed by Giles and Martelli (1971) from a

theory concerning the motion and spreading of inhomogeneities in a magneto-active plasma (Gurevich and Tsedilina, 1967). This theory does not suffer from the same altitude limitations as the Haerendel theory, and in certain circumstances might be applicable to an ion cloud which was contained within the neutral cloud for the whole of its lifetime.

A barium cloud which was released over South Uist at 129km., and which consequently did not separate into neutral and ionised components, has provided an opportunity to apply this alternative theory and discover whether the electric field value thus obtained is comparable with those measured under similar conditions in other experiments.

A brief outline of the theory used in this study will be given in chapter two, and its predictions and range of applicability will be compared with those of the Haerendel theory. The results of the study of this non-separated cloud will be given in chapter four.

In section 1.3 it has been mentioned that by measuring neutral winds during magnetic disturbance, the mechanisms which alter the quiet time wind system can be studied. The two mechanisms which might operate are ion drag of the neutral atmosphere and heating of the auroral ionosphere, both of which are likely to be enhanced during a magnetic storm. The main aim of the neutral wind studies made by our group has been to determine which of these two mechanisms predominates.

To this end a large number of neutral clouds released over Kiruna have been considered. These have been released both by our own group and by a group from the Max Planck Institut,

Garching. Some of these clouds were produced during magnetically quiet periods, and thus could be used to test the neutral wind model of Kohl and King (1967). Others, produced during magnetically disturbed phases, were studied in relation to associated ion cloud and quiet time neutral cloud results, in order to discover whether enhanced ion drag or enhanced ionospheric heating best explained the neutral winds observed at such times. Similarly, two clouds released over South Uist were studied in an attempt to fit the observed effect of magnetic disturbance on neutral winds at sub-auroral latitudes into the general picture.

An outline of the neutral wind model of Kohl and King will be given in chapter two, and the results of the neutral cloud studies will be given in chapter five.

In chapter three, information will be given concerning the release and observation of the clouds studied, and the subsequent data analysis.

Chapter Two

THEORETICAL MODELS OF ION CLOUD AND NEUTRAL PARTICLE MOTIONS

2.1 Ion cloud models

Experiments using the barium cloud technique for measuring ionospheric electric fields have been interpreted with the aid of a theoretical model developed for this purpose by Haerendel, Lüst and Reiger (1967). This model describes the motion of an ion cloud, treated as a finite cylindrical inhomogeneity in the ionosphere, under the influence of electric and magnetic fields, and is used to deduce from this motion the value of the electric field acting perpendicular to the magnetic field lines. A basic assumption of this theoretical model is that the cylindrical shape of the ion cloud, and its density, are conserved throughout its motion.

It is evident from observations of several ion clouds (see for example figs. 2.1 and 2.2) that this condition is not always adhered to, and in some cases considerable deformation and density variation occur during the lifetime of a cloud. Gurevich and Tsedilina (1967) have studied the theory of the motion and spreading of an inhomogeneity in a plasma, and predict that in certain circumstances considerable deformation of the inhomogeneity will occur. Thus this model would appear to be of value in the analysis of certain ion cloud releases, although at the expense of some restrictions not imposed by the Haerendel model.

Both models are derived using the same basic equations, which are set out in the following section. The difference

between the two models is in the initial shape assumed for the ion cloud and the consideration of subsequent deformation. Thus the two models involve different sets of simplifying assumptions. Inevitably, these simplifying assumptions impose limits on the applicability of each theory. It is the comparison of such limitations on the two models which is the major consideration here.

2.2 Basic equations for ion cloud models

In both ion cloud models a 3-fluid plasma is considered; i.e. electrons, one species of singly charged positive ions and one neutral species. A set of 3 momentum transfer equations is therefore required to describe this system, and these are given by

$$N_k m_k \frac{d\underline{v}_k}{dt} = N_k \underline{F}_k + \underline{c}_k - \nabla p_k \qquad (2.1)$$

where the subscript k is replaced by e (electrons), i (ions) or n (neutrals) when the set is written out in full. N_k, m_k and $\underline{v}_k$ are number density, mass and mass velocity, and the terms on the right hand side of the equation are a force term, a collision term and a pressure gradient term.

The vector force $\underline{F}_k$ is assumed to be given by

$$\underline{F}_k = q_k(\underline{E} + \underline{v}_k \times \underline{B}) + m_k \underline{g}$$

where q_k is electric charge, and $\underline{E}$, $\underline{B}$ and $\underline{g}$ are the electric, magnetic and gravitational fields respectively.

The collision term $\underline{c}_k$ is taken to be

$$\underline{c}_k = N_k \sum_l m_k \nu_{kl} (\underline{v}_l - \underline{v}_k)$$

where the collision frequency ν_{kl} has been defined to include the reduced mass term which normally appears in expressions of this type.

The following simplifying assumptions are now made:

a) all processes are assumed to be quasi-stationary, so the

left hand side of equation 2.1 can be set equal to zero.

b) the gravitational force term is neglected, implying that the atmospheric scale heights are large compared with the extension of the cloud.

c) the magnetic field is assumed to be homogeneous and constant with time.

d) collisions between electrons and ions are neglected in comparison with collisions of either of these with neutral particles. This assumption further implies that the velocity of the neutral particles can be taken to be constant with time.

e) all processes are assumed to proceed isothermally, and thus the pressure is given by

$$p_k = N_k k T \qquad \text{where all } T_k = T.$$

Equation 2.1 thus reduces to the two equations of motion, for ions and electrons

$$N_k e(\underline{E} + \underline{v}_k \times \underline{B}) + N_k m_k \nu_{kn}(\underline{v}_n - \underline{v}_k) - \underline{\nabla} N_k k T = 0 \qquad (2.2)$$

These are solved together with Maxwell's equations and the continuity equations for ions and electrons. Of Maxwell's equations only

$$\text{curl } \underline{E} = 0 \qquad (2.3)$$

need be explicitly included, this being consistent with assumption (a) above.

The continuity equations are given by

$$\frac{\partial N_k}{\partial t} + \underline{\nabla}.(N_k \underline{v}_k) = 0$$

since production and loss processes are neglected. Because the Debye length (1 cm.) is small compared with the distances being considered we must assume charge neutrality and put $N_i = N_e = N$. From this we have $\underline{\nabla}.\underline{j} = 0$, where $\underline{j} = eN(\underline{v}_i - \underline{v}_e)$.

The vector $\underline{j}$ represents the difference between the two

continuity equations, thus they are not independent, and only

$$\frac{\partial N}{\partial t} + \underline{\nabla}\cdot(N\underline{v}_i) = 0 \qquad (2.4)$$

remains.

Equation 2.2 can now be solved to obtain an expression for $\underline{v}_k$. We will work in the rest frame of the neutral particles, using primed symbols to denote quantities in this frame.

Using the following definitions

$$\underline{v}'_k = \underline{v}_k - \underline{v}_n$$

$$\underline{E}' = \underline{E} + \underline{v}_n \times \underline{B}$$

$$\underline{e}_B = \frac{\underline{B}}{B}$$

$$\gamma_k = \frac{q_k B}{m_k \nu_{kn}}$$

$$\mu_k = \frac{kT}{q_k}$$

$$\underline{u}_k = \frac{1}{B}\left(\underline{E}' - \mu_k \frac{\underline{\nabla} N}{N}\right)$$

we arrive at

$$\underline{v}'_k = \gamma_k \underline{u}_k + \gamma_k \underline{v}'_k \times \underline{e}_B$$

from which we have, by substituting this expression for $\underline{v}'_k$ into the right hand side of the same expression

$$\underline{v}'_k = \gamma_k \underline{u}_k + \gamma_k^2 \underline{u}_k \times \underline{e}_B + \gamma_k^2 (\underline{v}'_k \times \underline{e}_B) \times \underline{e}_B \qquad (2.5)$$

Equation 2.5 can be re-written as

$$\underline{v}'_k = \frac{\hat{\sigma}}{N q_k}\left(\underline{E}' - \mu_k \frac{\underline{\nabla} N}{N}\right) \qquad (2.6)$$

where $\hat{\sigma}$ is the conductivity tensor. In a co-ordinate system where the z-axis is parallel to $\underline{B}$ (which we may call the magnetic co-ordinate system), the tensor $\hat{\sigma}$ can be expressed as a matrix operator

$$\hat{\sigma} = \begin{pmatrix} \sigma_P & -\sigma_H & 0 \\ \sigma_H & \sigma_P & 0 \\ 0 & 0 & \sigma_\parallel \end{pmatrix}$$

where σ_P, σ_H and $\sigma_\parallel$, respectively the Pedersen, Hall and parallel conductivities, are given by

$$\sigma_P = \frac{N q_k}{B}\left(\frac{\gamma_k}{1 + \gamma_k^2}\right)$$

$$\sigma_H = -\frac{N q_k}{B}\left(\frac{\gamma_k^2}{1+\gamma_k^2}\right)$$

and $$\sigma_{\parallel} = \frac{N q_k}{B}\cdot\gamma_k$$

The diffusion operator $\hat{\delta}$, where $\hat{\delta}$ is the tensor of the difference between the diffusion coefficients for ions and electrons, is given similarly by

$$\hat{\delta} = \frac{\mu_k}{N q_k}\hat{\sigma}$$

Then, going back to the rest frame of the observer, we have from equation 2.6

$$\underline{v}_k = \frac{\hat{\sigma}}{N q_k}\cdot(\underline{E} + \underline{v}_n \times \underline{B}) - \frac{\hat{\delta}\,\nabla N}{N} + \underline{v}_n \qquad (2.7)$$

Thus the basic equations, which are required to describe the motion of an ion cloud within the limitations of the assumptions made so far, are 2.3, 2.4 and the pair of equations 2.7 for ions and electrons.

2.3 Comparison of the two ion cloud models

In the Haerendel model a solution is obtained to the set of basic equations by making further simplifying assumptions. Firstly it is assumed that the term representing the ambipolar diffusion of the cloud in equation 2.7 $(\frac{\hat{\delta}\nabla N}{N})$ can be neglected. This implies that the irregularity conserves its shape throughout its motion, since the ambipolar diffusion is a result of the difference in mobilities of ions and electrons. This assumption is justified by invoking a short-circuiting mechanism, as shown in fig. 2.3, in order to minimize the charge separation.

In place of the conductivity tensor $\hat{\sigma}$, the term λ^* (the ratio of the integrated Pedersen conductivities along field lines which pass through and outside the cloud) is now used, as this is the dominant conductivity consistent with the assumptions made so far.

For the cloud to conserve its shape, λ^* must be constant.

This condition is only fulfilled during the early stages of the cloud's motion, the precise time for which it is true depending on the altitude of the cloud. Thus a limitation is imposed that the cloud's altitude must be such as to allow a reasonable length of observation time, but without invalidating the constraint on λ^*. This limitation means that at 180 km. for example, about fifteen minutes of useful observation is possible and at 150 km. about five minutes. Below 150 km. the time for which observations can usefully be made quickly becomes unacceptably short.

The equation finally arrived at in the Haerendel theory, for the electric field perpendicular to the magnetic field lines is

$$\underline{E}_\perp = \frac{1+\lambda^*}{2} B \left[\underline{e}_B \times \underline{v}_\perp + \frac{1}{\gamma_i} (\underline{v}_\perp - \underline{v}_{n\perp}) + \frac{\lambda^* - 1}{\lambda^* + 1} \underline{v}_{n\perp} \times \underline{e}_B \right]$$

and this equation can be applied to clouds which conserve their shape and are above about 150 km., for the reasons stated above.

The model of Gurevich and Tsedilina imposes the further limitation on the basic equations that the ion cloud should represent only a weak perturbation in the ambient plasma (although this limitation is removed in certain restricted solutions of the model by Kaiser (1968), Kaiser et al. (1969) and Giles and Martelli (1971)). The basic equations are solved in terms of the Fourier components of the plasma perturbation. It is found that the theory predicts that the perturbation will tend to separate into two distinct local density maxima, each moving with a different velocity. The degree of separation which will occur depends both on ambient conditions and on the extent to which the initial perturbation is aligned with the magnetic field. Basically,

that part of the inhomogeneity which is initially highly field aligned will later be found (still field aligned) in one density maximum, while the second maximum will comprise the initially non field aligned parts of the inhomogeneity. The motion of the field aligned maximum is electron controlled, and that of the non field aligned maximum is ion controlled.

Gurevich and Tsedilina derive expressions for the velocities of the two maxima in terms of ionospheric parameters. Giles and Martelli (1971) apply this theory to the motion of artificial ion clouds, without imposing any further limitations, and derive expressions for the ionospheric electric field and the neutral wind velocity using the velocities of the two maxima. The expressions derived are

$$\underline{E}_\perp = \underline{B} \times \underline{v}_1 + \xi \underline{B} (\underline{v}_2 - \underline{v}_1) + \eta (\underline{v}_2 - \underline{v}_1) \times \underline{B} \qquad (2.8)$$

$$\underline{v}_n = \underline{v}_2 + \chi (\underline{v}_1 - \underline{v}_2) \cdot \underline{e}_B \qquad (2.9)$$

where $\underline{v}_1$ is the velocity of the field aligned maximum, $\underline{v}_2$ is the velocity of the non field aligned maximum and ξ, η and χ are constants involving ion and electron collision frequencies and gyro-frequencies. Values of these constants at various altitudes are shown in table 2.1.

Equation 2.8 applies at all altitudes, and takes into account possible deformation of the ion cloud. It can be adapted for application in circumstances where the ion cloud does not separate into two distinct maxima, and where the ion cloud does not separate from the neutral cloud (Giles and Martelli, 1971). In addition, the expression for $\underline{E}_\perp$ does not require measurement of $\underline{v}_n$, the neutral wind velocity; indeed $\underline{v}_n$ can be calculated from measured values of $\underline{v}_1$ and $\underline{v}_2$,

using equation 2.9, thus an independent check can be made on the applicability of this theory to an ion cloud release, by comparing observed and calculated neutral wind values. However, it must be remembered that this theory is derived on the assumption that the inhomogeneity represents only a weak perturbation to the ambient plasma, and this will not necessarily be the case for an ion cloud.

In general, the Haerendel model is the appropriate one to apply to clouds which conserve their shape and are above 150 km , since it requires only a limited knowledge of ionospheric parameters. (Only δ_i, the ratio of the gyro-frequency to the collision frequency for ions, is required in the Haerendel equation for $E_\perp$, since at all relevant altitudes $\lambda \sim 1$.) However, at lower altitudes or where there is no separation of neutral and ionised clouds, The model of Gurevich and Tsedilina can be expected to give more reliable results, although greater knowledge of the values of ionospheric parameters is required.

2.4 Neutral wind theory

The world wide movement of neutral particles in the upper atmosphere has been studied by various workers since the 1950s. As a result of these studies it has been suggested that the neutral wind may cause ionospheric drifts which could account for many of the experimentally observed F-layer anomalies.

Initially, theoretical neutral wind studies concentrated on one region, or one observed anomaly, rather than attempting to set up a global wind model. Thus King (1964) proposed a wind system which might account for the ionospheric seasonal anomaly; Hines (1965) derived an expression for horizontal

wind velocity to explain the observation by King-Hele (1964) of the eastward rotation of the atmosphere; and Geisler (1966) calculated values for the neutral wind at the latitude of 45°.

More recently, Kohl and King (1967) have set up a global neutral wind model based on the exospheric temperature distribution proposed by Jacchia (1965). In this model, the neutral wind is assumed to result from a pressure gradient which occurs because of the difference in temperature, and hence in atmospheric density, between the dayside and nightside of the globe. Fig. 2.4 shows the exospheric temperature dsitribution on which this model is based (Jacchia 1965). It will be seen from this diagram that the highest temperatures, and hence pressures, occur at about 14.00 local time, and the lowest temperatures at 04.00 local time. Therefore the pressure gradient sets up a wind system which, in general, transports neutral particles from regions near the pressure maximum to regions near the pressure minimum. However, Coriolis and inertial forces also influence the wind system, with the result that the entire pattern is shifted slightly towards later local times than would be expected if the system were based only on the effects of solar heating (see for example fig. 2.5).

The global wind model of Kohl and King takes into account the following factors:

1) the pressure gradient ∇p, where p is the atmospheric pressure. This arises from solar heating, as described above.
2) the Coriolis force $2\rho(\underline{v}_n \times \underline{\omega})$, where ω is the angular frequency of the earth's rotation, $\underline{v}_n$ is the atmospheric

wind velocity and ρ the atmospheric density.

3) the viscous force $\rho\mu(\partial^2 \underline{v}_n/\partial h^2)$, where μ is the kinematic coefficient of viscosity and h is altitude.

4) the inertial force $\rho[\partial^2 \underline{v}_n/\partial t + (\underline{v}_n \cdot \nabla)\underline{v}_n]$.

5) the ion drag effect of collisions between neutral particles and ions given by

$$\rho \nu_n (\underline{v}_n - \underline{v}_i) = \frac{\rho \nu_i N_i}{N_n}(\underline{v}_n - \underline{v}_i)$$

where ν_n and ν_i are neutral and ion collision frequencies, N_n and N_i are neutral and ion concentrations and $\underline{v}_i$ is the ion velocity.

Certain constraints are placed on the model, either implicitly in the expressions used above, or as a result of subsequent simplifying assumptions.

The inertial force term is simplified by assuming that local distortions such as turbulence do not occur. This means that the second term in the expression is small compared with the first, and may be neglected. Rüster and Dudeney (1972) have obtained a solution to the equation of motion of the neutral atmosphere including an approximate form of the $(\underline{v}_n \cdot \nabla)\underline{v}_n$ term. This solution shows that the term is of importance at middle latitudes, but not significantly so at high latitudes.

The ion drag term implies the assumption that ν_i is smaller than the ion gyro-frequency and this is only true above E-layer heights.

Electric fields are not taken into account in the model, so the ion motion is mainly in the direction of the earth's magnetic field and the ion velocity is taken to be

$$\underline{v}_i = (\underline{v}_n \cdot \underline{e}_B)\underline{e}_B \quad , \qquad \text{where} \quad \underline{e}_B = \frac{\underline{B}}{B}$$

The equation of motion for the neutral atmosphere

therefore becomes

$$\frac{\partial \underline{v}_n}{\partial t} - \mu \frac{\partial^2 \underline{v}_n}{\partial h^2} - 2(\underline{v}_n \times \underline{\omega}) + \nu_i N_i \underline{v}_n - (\underline{v}_n \cdot \underline{e}_B)\underline{e}_B = -\frac{1}{\rho} \nabla p + g \quad (2.10)$$

and this can be solved for $\underline{v}_n$ if the appropriate values of N_i, μ, ν_i/N_n and $\nabla p/\rho$ are known. Kohl and King computed numerical solutions of this equation and obtained values for the horizontal components of $\underline{v}_n$ for different latitudes, altitudes and local times. Two of the sets of vectors thus obtained, for the northern hemisphere and for an altitude of 300 km., are shown in figs. 2.5 and 2.6. Fig. 2.5 represents sunspot maximum or day-time conditions, and fig. 2.6 represents sunspot minimum or night-time conditions.

The wind velocities shown in these diagrams apply above E-layer heights, in the absence of local distortions in the neutral atmosphere, and in the absence of ionospheric electric fields (i.e. in magnetically quiet conditions). These are the most important limitations on the theory, but additional limitations imposed in order to obtain numerical solutions to equation 2.10, must be borne in mind. These are

1) the solutions obtained are more applicable to equinox conditions than to solstice conditions.
2) the solutions are not reliable close to the equator since magnetic and geographic equators have been assumed to coincide.
3) certain local inaccuracies may result from the assumption that electron density, scale height etc., are independent of time and latitude.

Height (km)	ξ	η	$\varkappa$
80	1×10^{1}	1×10^{2}	8×10^{-2}
90	5×10^{-2}	3×10^{1}	2×10^{-2}
100	3×10^{-3}	8×10^{-2}	3×10^{-2}
110	8×10^{-4}	5×10^{-3}	1×10^{-1}
120	7×10^{-5}	1×10^{-5}	6×10^{-1}
130	1×10^{-5}	-1×10^{-5}	1.7×10^{0}
140	5×10^{-7}	-1×10^{-7}	3.4×10^{0}
150	0	0	6.5×10^{0}
160	0	0	1.1×10^{1}
170	0	0	1.7×10^{1}
180	0	0	2.7×10^{1}
190	0	0	4.0×10^{1}
200	0	0	6.8×10^{1}

Table 2.1 Estimated values of the constants ξ, η, and $\varkappa$ at different altitudes

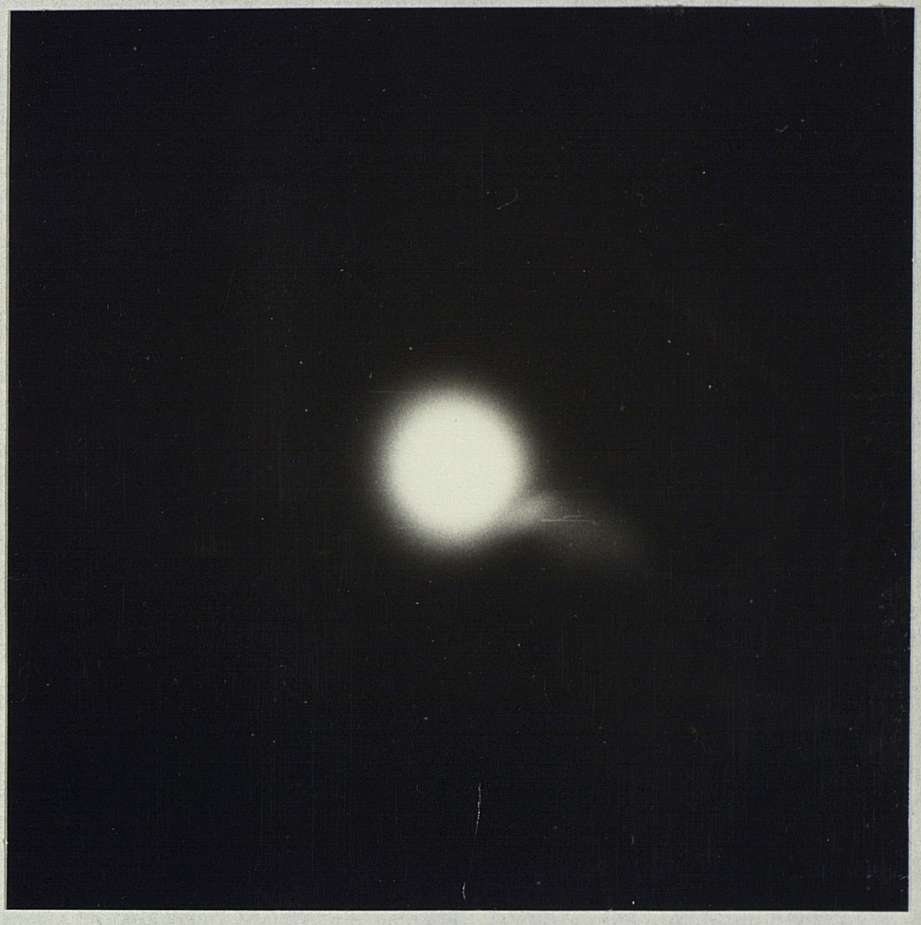

Figure 2.1 Cloud P11K 200 seconds after release

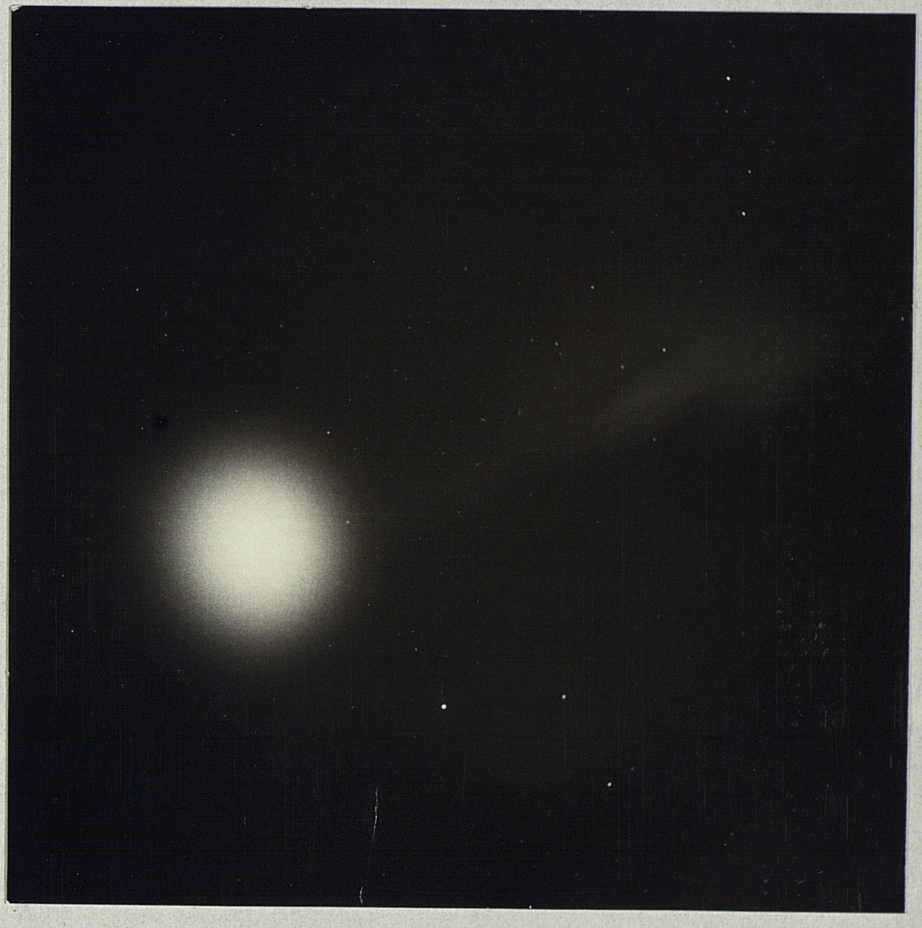

Figure 2.2 Cloud P11K 500 seconds after release, showing change in shape of ion cloud, by comparison with Fig. 2.1, during early stages of its lifetime

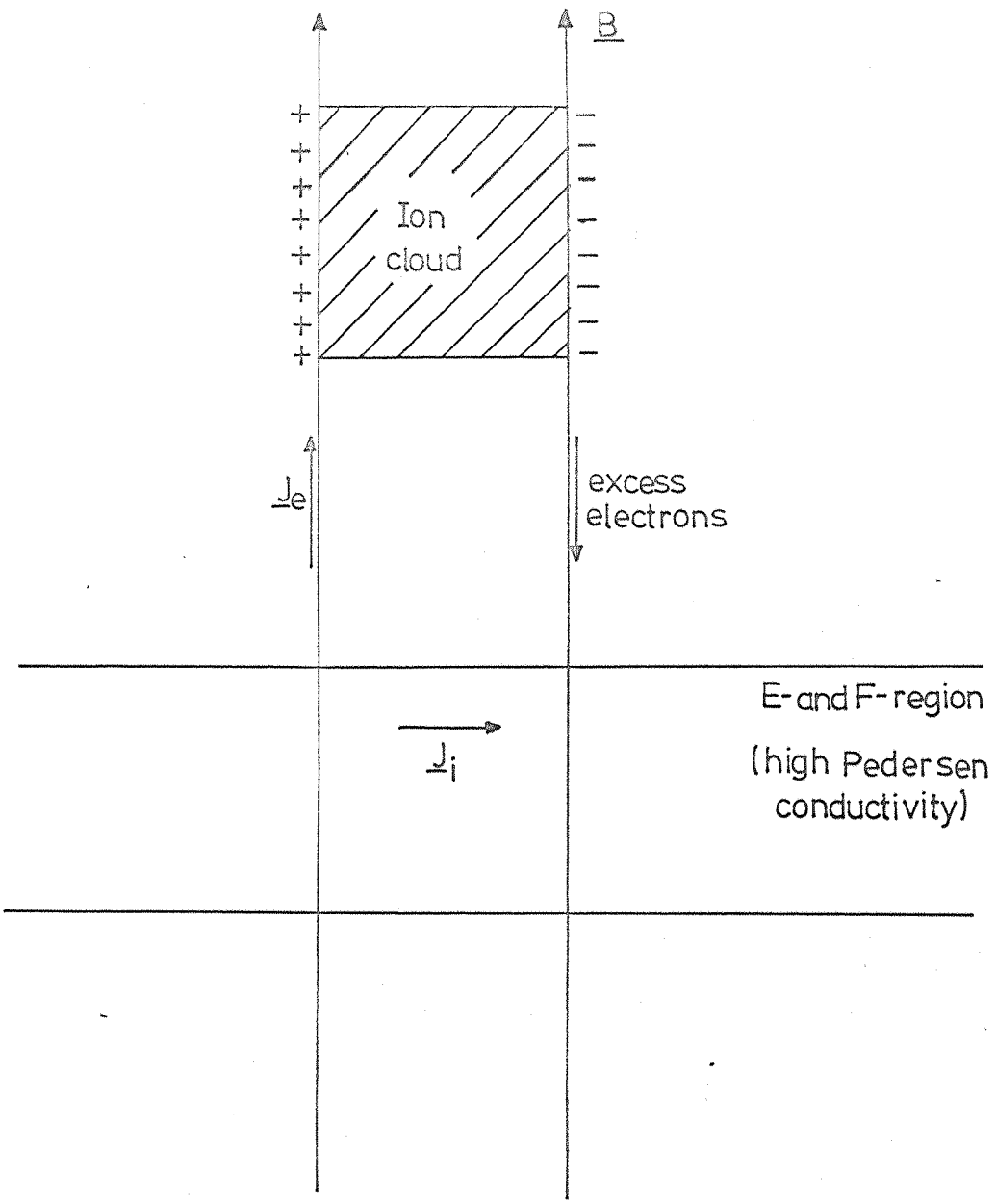

$\underline{J}_e$ — electron current

$\underline{J}_i$ — ion current

Figure 2.3 Short-circuiting mechanism

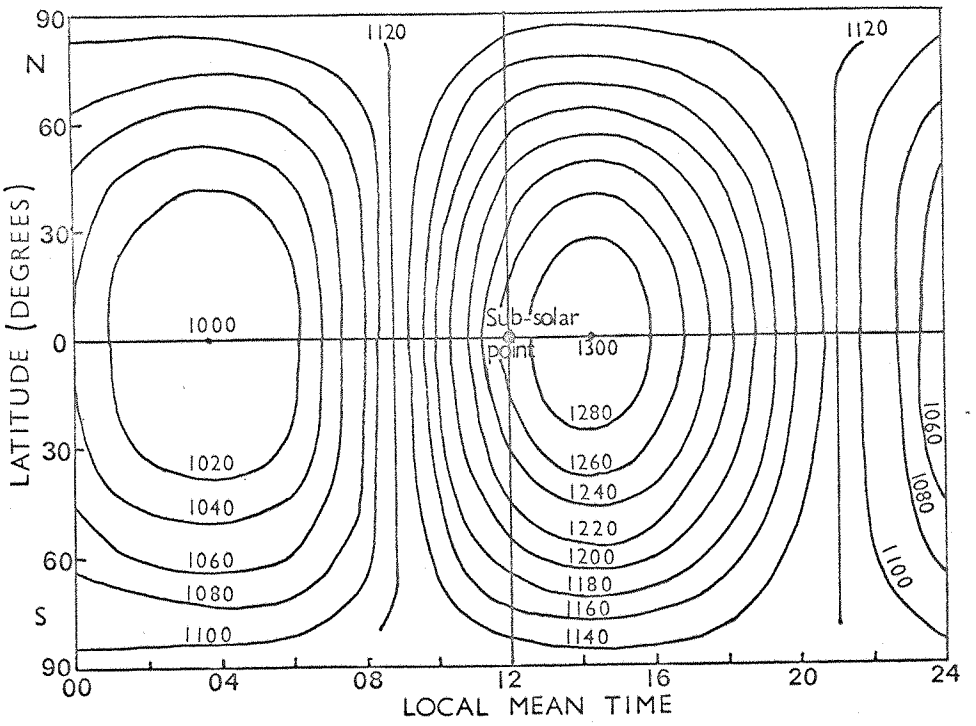

Figure 2.4 Equinox exospheric temperature distribution for medium solar cycle conditions. The isothermal contours are approximately concentric circles around the atmospheric bulge which occurs on the equator at 14.30 L.M.T. (after Jacchia, 1965).

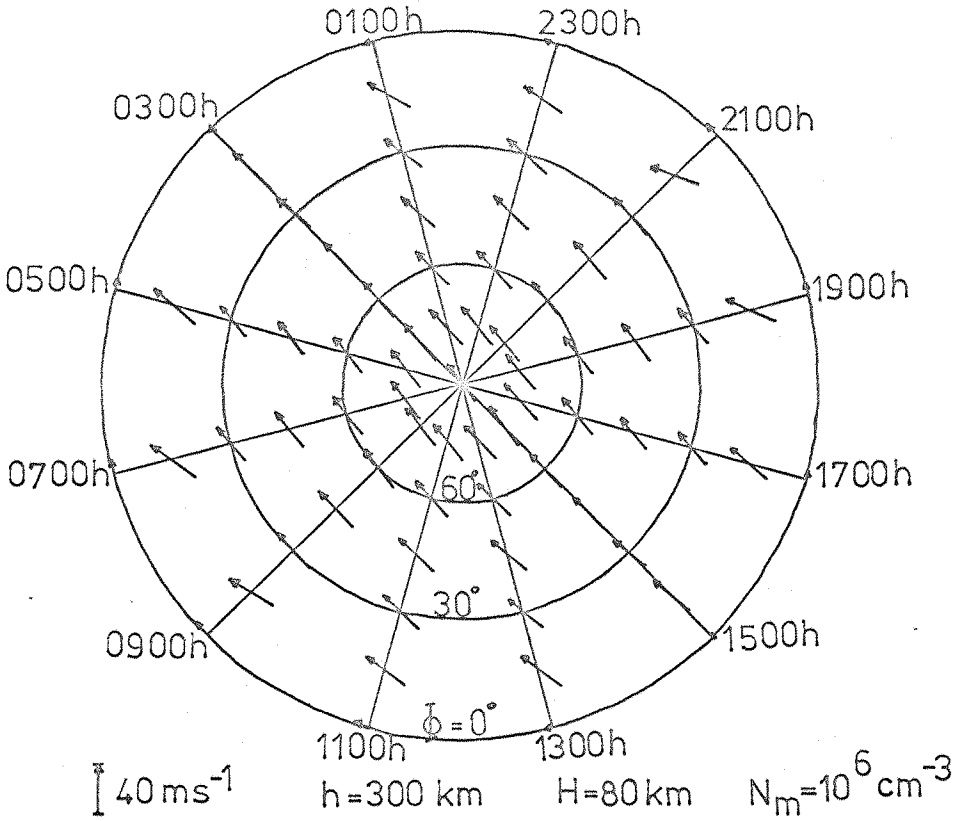

Figure 2.5 The atmospheric wind system in the northern hemisphere calculated for an altitude of 300 km when the peak electron density is $10^6 cm^{-3}$ (After Kohl and King, 1967.)

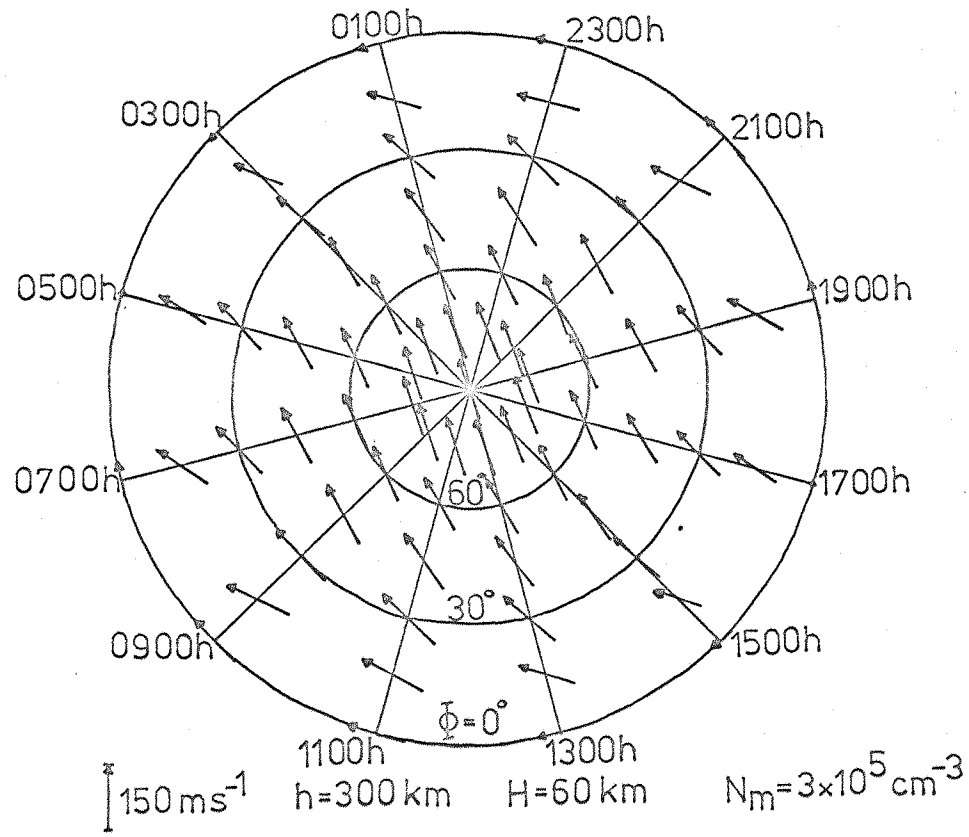

Figure 2.6 The atmospheric wind system in the northern hemisphere calculated for an altitude of 300 km when the peak electron density is $3 \times 10^5 cm^{-3}$ (After Kohl and King, 1967.)

Chapter Three

EXPERIMENTAL DETAILS AND DATA ANALYSIS

3.1 The experiments

Data from nine chemical release experiments has been used in this thesis. Four of these experiments were carried out in a collaborative program by our own group from Southampton and Sussex Universities. The design, preparation and launching of payloads was the responsibility of the group at Sussex University, and observations and data analysis were carried out by the Southampton University group. Of these four experiments, one has been used to investigate the applicability of an alternative theory of ion cloud motion in deducing electric fields. This experiment was launched from South Uist, Outer Hebrides. Details will be found in chapter four.

The other three of our experiments, launched from ESRANGE, Kiruna, form part of a study of neutral winds in magnetically quiet and disturbed conditions. Data for this study was also obtained from our own photographic records of five releases made by other experimenting groups, and observed by us at their invitation. Three of these releases were made in Kiruna and two in South Uist. Information on the eight experiments used in this study is given in table 3.1.

Most of the payloads consisted of one or more canisters of pressurised copper oxide and barium granules (barium thermite). In some cases strontium thermite was used, to produce wholly neutral vapour clouds. Two barium shaped charges were also released, one in each experiment

performed by the Max Planck Institut group. Details concerning the construction of payloads have been given by Hunter (1970) and Hilmi (1974), and these references also include explanation of the shaped charge technique.

3.2 The observation sites and equipment

In choosing observation sites, a compromise has to be reached between achieving a suitable triangulation base and well distributed sites, and adapting to the limitations of the locality and the available manpower. Communication between the observation sites and the launch site is essential, and because of the remoteness of rocket ranges this often means that the observation sites cannot be ideally situated from the point of view of triangulation accuracy. Fig. 3.1 shows the Kiruna rocket range and the observation sites used. For some launches it was decided that it would be preferable to use fewer observation sites, thus making more cameras available at each site so that a wider variety of information could be obtained. The positions of the observation sites used in conjunction with the launches from the South Uist range are shown in fig. 3.2.

The basic observational equipment at each site consisted of Hasselblad 500EL cameras and associated timing units. The Hasselblad 500EL is a motor driven camera which takes 70 mm. film. This large film size is desirable since much of the measurement is made directly on the negatives and the accuracy attainable with 35 mm. negatives is insufficient. The crystal oscillator controlled timing units, designed specifically for these experiments, provide to the cameras a series of pulses which cause regular exposures of known duration. Several choices of length and frequency of

exposure are available, the choice of length of exposure ranging from one to twenty seconds, and of frequency one to four per minute.

The basic triangulation data was obtained in every case from Hasselblads fitted with Zeiss Planar 2.8/85 mm. lenses, and loaded with high speed black and white film. This type of lens gives a 52^{o} field of view.

Various additional data was obtained in several cases, this data falling into three categories.

1) Some 35 mm. colour film was taken, partly because the red/magenta ionised clouds and the blue/green neutral clouds are easy to distinguish on this type of film, and partly because it provides suitable data for a quick initial analysis.
2) Some Hasselblads fitted with Zeiss Sonnar 4/150 mm. lenses were used, to obtain greater magnification for detailed study (though at the expense of a much reduced field of view, which limits considerably the number of identifiable stars in the reference background).
3) Both 35 mm. and 70 mm. film was obtained, from cameras fitted with narrow band interference filters. These filters were used in an attempt to separate photographically the neutral and ionised components of the clouds.

The distribution of observational equipment for the various launches is given in tables 3.2 - 3.7.

3.3 Operation of an observation site

There are two considerations which are of major importance in obtaining good triangulation data from a photographic observation site. These are, firstly, that the exact time at

which each photograph is obtained should be known and, secondly, that all parts of the clouds should be in the field of view of the cameras at all times.

To obtain accurate times for all photographs, each observation site is in contact with the launch site, by telephone or radio telephone. All timing units which control the operation of motor driven cameras are synchronised before the launch occurs, and the synchronisation is checked at the end of the observation period so that allowance can be made if necessary for any fast or slow running of a timing unit. It is useful if, during the period of observation, a tape recording of the proceedings is made at each observation site. This can be used to check that no exposures have been missed due to malfunction of a timing unit or camera, since the winding-on of a motor driven camera is clearly audible on a tape recording. In addition, comments concerning the development of the clouds, the functioning of the observational equipment, the stars which are in the field of view, can be valuable in helping to attribute a time to any particular photograph and in speeding up the work of data analysis.

Before any experiment is launched, the heights at which clouds are to be released have been chosen, and these are used in calculating the azimuth and elevation settings for the cameras at each site, so that the clouds should be in the field of view on release. A check is made as soon as the release is visible, and the camera settings are adjusted if necessary. Subsequent adjustments are made as the cloud moves, but it is inadvisable to alter settings too frequently if this can be avoided, since star identification

during data analysis can be a lengthy process if the field of view changes constantly from one frame to the next.

3.4 Data analysis

As mentioned briefly in chapter one, the motion of an artificial cloud is determined by triangulation against the fixed star background. For this process to be carried out, photographs taken simultaneously from two or more camera sites must be available. The actual procedure for triangulation is described by Groves and Owen (1960) and Groves, Owen and Thorpe (1960). The computer program for carrying out this procedure was given to the Southampton/ Sussex group by Dr. Groves, and has been adapted to meet our particular requirements. The main adaptation has been the splitting of the program into two sections to facilitate data handling in the computing system available to us.

In the first section of the analysis, the x-y co-ordinates of several stars relative to an arbitrary zero are measured on each frame, or 'plate', and a best fit procedure is used to relate these co-ordinates to the true right ascension and declination of the stars at the time of exposure of the frame. The errors in the fit of the x and y co-ordinates of each point are also calculated during this process and, to attain a suitable degree of accuracy, any star for which the error in either co-ordinate exceeds a predetermined limit, is rejected. The fitting procedure is then repeated so that eventually a best fit is obtained for which no error exceeds the limit.

The output of this section of the program is a set of nine numbers for each frame, known as the plate constants. These define the direction of the line of sight

perpendicular to the plate, the orientation of the plate about this line of sight, and a scaling factor related to the magnification.

In the second part of the analysis, the x-y co-ordinates of selected points on the clouds are measured, and the plate constants are used to calculate the directions of the lines of sight to each of these points, from two or more camera sites. The position of each cloud point is thus given by the point of intersection of the appropriate lines of sight. In fact, certain errors in identifying and measuring points are inevitable and the lines of sight will not, in general, intersect. Therefore a least squares criterion is used to determine the position of the cloud point from the calculated lines of sight. The output from this part of the program is the three distances (north, east and vertical) of each cloud point from the launcher, and also the errors in these distances.

The measurements of x-y co-ordinates are made using a Benson-Lehner 'Oscar'. With this machine measurements can be made on slides (projected onto 'Oscar's' screen) or prints (fixed onto the screen). The measurement is made by setting x and y overlays to coincide over the required point, and the co-ordinates of the point are then printed out automatically.

It has been found from experience that measurements of stars are best made directly from negatives, used as slides, since this reduces the likelihood of identifying dust specks etc. as stars, these being virtually indistinguishable on prints. However, identification of cloud points is easier on prints than on slides, since magnification and contrast

can be enhanced by suitable printing.

In order that points measured on a print may be used in conjunction with the plate constants obtained using a slide, a set of four reference points is marked on each frame before printing. These are measured on both slide and print, and compared to determine the appropriate transformation for converting points measured on the print to equivalent points on the slide.

Designation	Place	Date	Time (U.T.)	Time (local)	
K-NA-16	ESRANGE, Kiruna.	15.3.69	17.55.00	18.55.00	
K-NA-17	ESRANGE, Kiruna.	16.3.69	18.05.00	19.05.00	
K-NA-18	ESRANGE, Kiruna.	17.3.69	18.11.00	19.11.00	
P11K	ESRANGE, Kiruna.	18.3.69	18.16.00	19.16.00	
P63K	ESRANGE, Kiruna.	21.4.71	23.03.30	24.03.30	
P54K	ESRANGE, Kiruna.	24.4.71	23.35.55	24.35.55	
SP3	R.A.Range, South Uist.	15.5.73	22.05.00	22.05.00	
SP4	R.A.Range, South Uist.	16.5.73	22.45.00	22.45.00	

M.P.I.-Max Planck Institut für Extraterrestrische Physik,
B.U.-University of Bochum.
S.S.-University of Southampton/University of Sussex.
A.W.R.E.-Atomic Weapons Research Establishment, Aldermaston.

(1)Both canisters of barium thermite released simultaneously.

Table 3.1 Details

	Payload composition	Release heights (km)	Experimenting group	3-hourly K_p index
	2 barium thermite 1 barium shaped charge	140 185 230	M.P.I.	4-
	5 strontium thermite	168 198 226 205 166	B.U.	1+
	2 barium thermite 1 barium shaped charge	145 195 250	M.P.I.	4+
	2 barium thermite	165	S.S.	1+
	1 barium thermite 1 strontium thermite	170	S.S.	6+
	1 barium thermite 1 strontium thermite	173 173	S.S.	0+
	1 barium thermite	152	A.W.R.E.	5+
	1 barium thermite	151	A.W.R.E.	6

Garching, Munich.

of experiments

Site	Camera	Exposure sequence	Film type	Comments
I Abisko[1]	Hasselblad 500 EL md[2]	5 secs, 2 per min	70mm, Tri X	
	Hasselblad 500 EL md	10 secs, 2 per min	70mm, HS Ektachrome	Exposure time increased to 15 secs for K-NA-16
II Observatory	Hasselblad 500 EL md	5 secs, 2 per min	70mm, HP3	
	Hasselblad 500 EL md	5 secs, 2 per min	70mm, FP4	HP3 film used for K-NA-16

(1) Site operated in conjunction with Dr. D.Rees of University College, London.

(2) md- Motor driven camera, operated automatically by camera timing unit.

Table 3.2 Allocation of cameras for launches K-NA-16, K-NA-17 and K-NA-18

Site	Camera	Exposure sequence	Film type	Comments
I Abisko[1]	Hasselblad 500 EL md[2]	5 secs, 2 per min	70 mm, HP3	
	Hasselblad 500 EL md	5 secs, 2 per min	70 mm, HS Ektachrome	
	Nikon 'F' md	20 secs, 1 per min	35 mm, 2475	4607Å filter fitted Camera failure
	Nikon 'F' md	20 secs, 1 per min	35 mm, 2475	4934Å filter fitted
II Observatory	Hasselblad 500 EL md	5 secs, 2 per min	70 mm, HP3	Observation period extended by increasing exposure and time interval later
	Hasselblad 500 EL md	5 secs 2 per min	70 mm, HP3	
	Asahi Pentax	20 secs, 1 per min	35 mm, 2475	4554Å filter fitted
III Downrange	Hasselblad 500 EL md	5 secs, 2 per min	70 mm, HP3	
	Hasselblad 500 EL md	5 secs, 2 per min	70 mm, HP3	Camera failure
IV Rangehead	Kodak Retinette	20 secs, 1 per min	35 mm, HS Ektachrome	

(1) Site operated in conjunction with Dr. D.Rees of University College, London

(2) md- Motor driven camera, operated automatically by camera timing unit.

Table 3.3 Allocation of cameras for launch P11K

Site	Camera	Exposure sequence	Film type	Comments
I Abisko	Hasselblad 500 EL md[1]	5 secs, 2 per min	70 mm, 2475	
	Hasselblad 500 EL md	5 secs, 2 per min	70 mm, 2475	'Telescopic'[2] lens
	Hasselblad 500 EL md	5 secs, 2 per min	70 mm, 2475	4554Å filter fitted Camera failure
	Nikon 'F' md	5 secs, 2 per min	35 mm, HS Ektachrome	No data obtained
II Observatory	Hasselblad 500 EL md	5 secs, 2 per min	70 mm, 2475	
	Hasselblad 500 EL md	5 secs, 2 per min	70 mm, 2475	'Telescopic' lens
	Hasselblad 500 EL md	5 secs, 2 per min	70 mm, 2475	4554Å filter fitted
IV Rangehead	Hasselblad 500 EL md	5 secs, 2 per min	70 mm, 2475	

(1) md- Motor driven camera, operated automatically by camera timing unit.

(2) A 150mm,f4 'telescopic' lens was fitted in place of the 85mm,f2.8 lens usually used.

Table 3.4 Allocation of cameras for launch P63K

Site	Camera	Exposure sequence	Film type	Comments
I Abisko	Hasselblad 500 EL md[1]	5 secs, 2 per min	70 mm, 2475	
	Hasselblad 500 EL md	5 secs, 2 per min	70 mm, 2475	4554Å filter fitted
	Hasselblad 500 EL md	5 secs, 2 per min	70 mm, 2475	4607Å filter fitted 'Telescopic'[2] lens
	Nikon 'F' md	5 secs, 2 per min	35 mm, HS Ektachrome	Film breakage after one frame
II Observatory	Hasselblad 500 EL md	5 secs, 2 per min	70 mm, 2475	
	Hasselblad 500 EL md	5 secs, 2 per min	70 mm, 2475	4554Å filter fitted
	Hasselblad 500 EL md	5 secs, 2 per min	70 mm, 2475	4607Å filter fitted 'Telescopic' lens No data obtained
IV Rangehead	Asahi Pentax	20 secs, 1 per min	35 mm, HS Ektachrome	

(1) md- Motor driven camera, operated automatically by camera timing unit.

(2) A 150mm,f4 'telescopic' lens was fitted in place of the 85mm,f2.8 lens usually used.

Table 3.5 Allocation of cameras for launch P54K

Site	Camera	Exposure sequence	Film type	Comments
I North Uist	Hasselblad 500 EL md[1]	5 secs, 2 per min	70 mm, HP3	
	Hasselblad 500 EL md	5 secs, 2 per min	70 mm, HP3	Camera failure
	Kodak Retinette	20 secs, 1 per min	35 mm, HS Ektachrome	
II Skye	Hasselblad 500 EL md	5 secs, 2 per min	70 mm, HP3	
	Ilford Sportsman	20 secs, 1 per min	35 mm, HS Ektachrome	
III South Uist	Hasselblad 500 EL md	5 secs, 2 per min	70 mm, HP3	
	Nikon 'F' md	20 secs, 1 per min	35 mm, 2475	Camera failure
	Nikon 'F' md	20 secs, 1 per min	35 mm, 2475	4934Å filter fitted
	Zeiss Contessa	20 secs, 1 per min	35 mm, HS Ektachrome	
IV Rangehead	Kodak Retinette	20 secs, 1 per min	35 mm, HS Ektachrome	Exposures made on alternate half minutes
	Asahi Pentax	20 secs, 1 per min	35 mm, HS Ektachrome	

(1) md- Motor driven camera, operated automatically by camera timing unit.

Table 3.6 Allocation of cameras for launch P38H

Site	Camera	Exposure sequence	Film type	Comments
V Bayhead[1]	Hasselblad 500 EL md[2]	5 secs, 4 per min	70 mm, 2475	
	Hasselblad 500 EL md	5 secs, 4 per min	70 mm, 2475	
VI Lochboisdale	Hasselblad 500 EL md	5 secs, 4 per min	70 mm, 2475	
	Hasselblad 500 EL md	5 secs, 4 per min	70 mm, 2475	

(1) A TV camera with image intensifier was also used at this site, and a video recording was made.

(2) md- Motor driven camera, operated automatically by camera timing unit.

Table 3.7 Allocation of cameras for launches SP3 and SP4

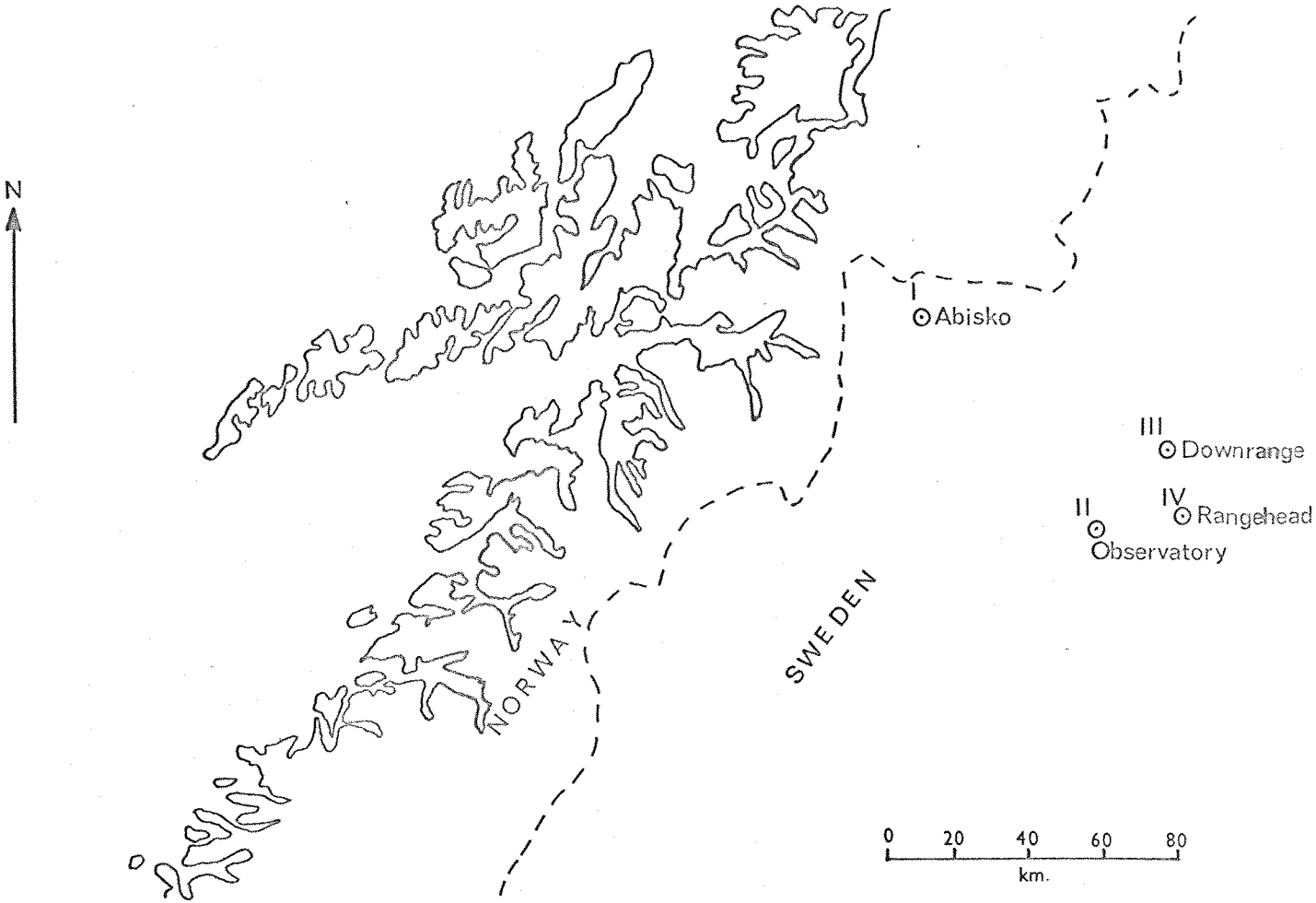

Figure 3.1 Map showing the observation sites used for the experiments in Kiruna

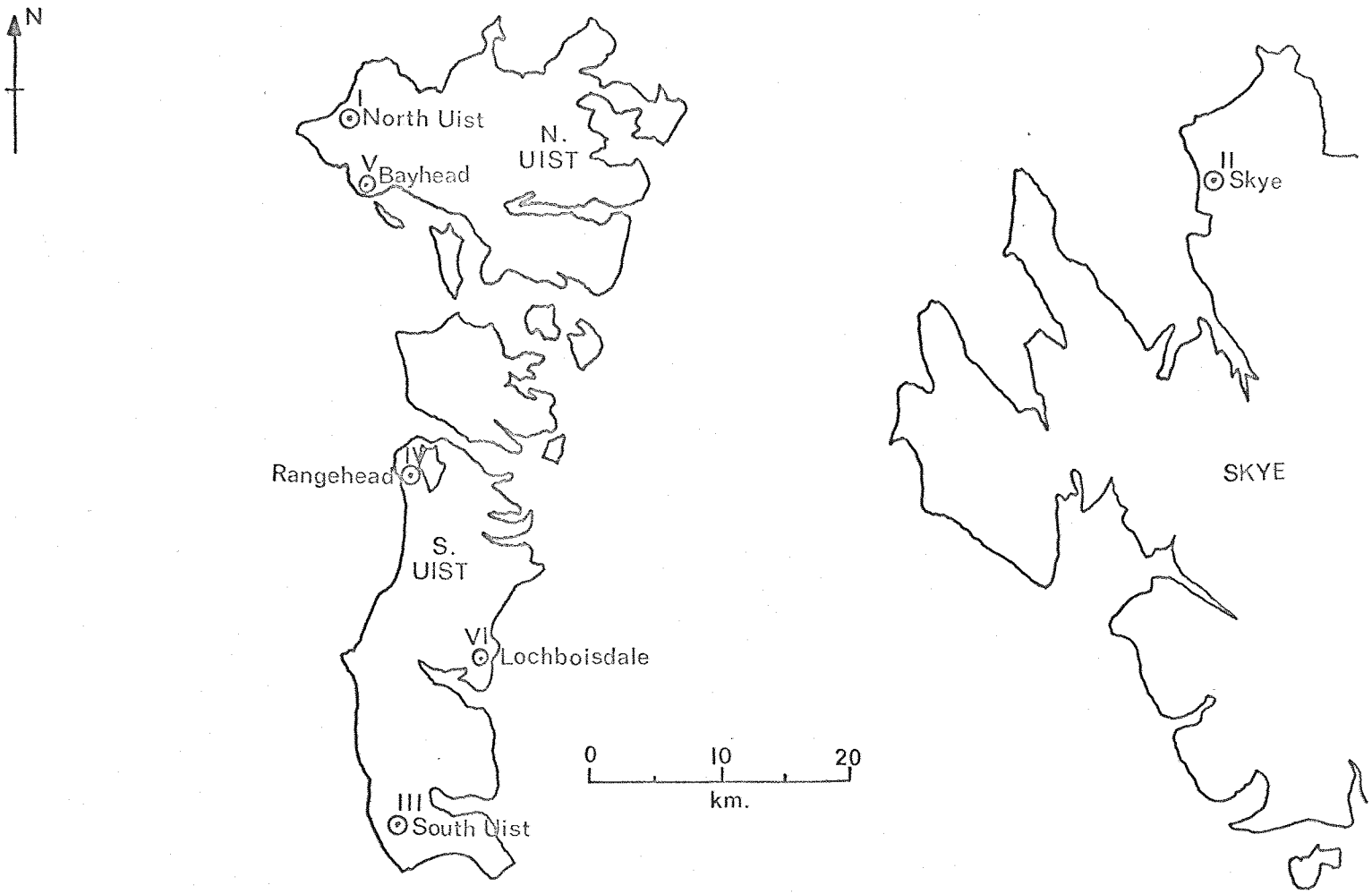

Figure 3.2 Map showing the observation sites used for experiments in South Uist

Chapter Four

INVESTIGATION OF THE USE OF AN ALTERNATIVE THEORY FOR ION CLOUD EXPERIMENTS

4.1 Experiment P38H

Experiment P38H was launched from R.A. Range, South Uist, Outer Hebrides ($57^{\circ}N, 7^{\circ}W$) on October 11th 1969 at 18.36.08 U.T. (19.36.08 B.S.T.). The payload consisted of two canisters of barium thermite, with a timing device and igniters, and was arranged to produce one cloud at apogee and a second on the downleg of the rocket's flight. However, apogee was rather low, and only one cloud was observed, this cloud being released at 129 km. Subsequent calculations suggested that a second cloud, if produced on the descent from this low apogee, would have been in the earth's shadow and therefore not visible.

The cloud was photographed from the four observation sites numbered I to IV in fig. 3.2. Observation conditions were good at all sites and the sky was clear throughout the observation period, with the exception of site II (Skye), where meteorological clouds obscured the release after seventeen minutes of observation. The distribution of observational equipment between the various sites is detailed in table 3.6.

The cloud was visible for approximately twenty minutes, after which time it had faded too far for photographs to be obtained.

4.2 Results of observation

Since the cloud was produced in the E-region, and magnetic conditions were quiet ($K_p = 2$), separation of neutral and

ionised components was not expected, and indeed did not occur. The cloud quickly developed into a crescent shape, which it maintained throughout the period of observation, as shown in fig. 4.1. The motion of the cloud was predominantly to the north, being slightly to the west of north during the first 600 seconds after release, and slightly east of north thereafter (see fig. 4.2) Because of the shape of the cloud, three points were chosen for triangulation. These were the 'top', 'centre' and 'bottom' of the cloud as shown in fig. 4.3, and although no objective criteria were used in identifying these points on successive photographs, very little difficulty was experienced in making a consistent subjective identification. The velocity components for the three cloud points are set out in table 4.1, both in geographic (z-axis vertical) and magnetic (z-axis $\parallel \underline{B}$) co-ordinate systems.

One camera at site III (South Uist) was fitted with a narrow band interference filter, nominally centered on the ionised barium line at 4934$\mathring{A}$. Photographs obtained through this filter contained an exposed region, faint but similar in shape to the cloud, which suggested that although there was no separation, there was a certain amount of ionisation and the cloud consisted of superimposed neutral and ionised components. However, this evidence must be viewed with caution for two reasons.

Firstly, there was no star reference background on these photographs, so no triangulation could be carried out to determine the position or motion of the observed ionisation. Subsequent investigation showed that the star background could not be photographed through filters of the type used

in this experiment. This is because the position of a star image on the film has changed due to the earth's rotation, before the light intensity received is sufficient to expose the film. This was found to be the case even when using the fastest film available and the largest possible camera aperture. Thus the cloud photographed through the filter could not be precisely related in position or size, to the cloud observed in non-filtered photographs.

Secondly, the wavelengths transmitted by a narrow band interference filter depend on the angle at which light is incident on it. If the exposure of the film was caused by light incident non-normally on the filter (due to poor alignment of the filter, for example) such light would not necessarily have a wavelength corresponding to the normal transmission curve of this filter. Thus, although the transmission curve does not include any of the wavelengths in the spectrum of neutral barium, this spectrum does include wavelengths which could be transmitted if incident non-normally on the filter. In the absence of any objective means of relating the photographs taken with and without the filter, the possibility of all such photographs showing the same neutral cloud cannot be ruled out.

4.3 Examination of possible causes of cloud shape

In view of the limited amount of information provided by this release, the major feature of interest was the crescent shape developed by the cloud, and the investigation of possible causes of this effect. Three possibilities have been considered as being responsible for the development of a crescent shape cloud. These are

1) wind shear

2) optical thickness

and 3) differential velocities of superimposed neutral and ionised cloud components.

4.3.1 Wind shear

It is well known that there are considerable vertical variations in neutral wind direction and velocity. Rees (1971), for example, has plotted vertical wind profiles for the height range 80 to 160 km. over Kiruna under various conditions. These profiles were derived from neutral chemical release experiments. From these and other experiments (Manring et al. 1964, Kochanski 1964) it is clear that major neutral wind variations occur at altitudes of up to about 120 km., and smaller variations occur at higher altitudes. Thus the release height of 129 km. for the cloud considered here is rather above the region of major neutral wind variation, but wind shear due to smaller variations could have affected its shape. The wind profile necessary to produce the cloud shape initially has been calculated, and is shown in fig. 4.4. This profile is not unreasonable for the altitude and conditions obtaining. However, although this wind profile would initially produce the observed crescent shape of the cloud, subsequently it could be expected to shear the cloud further, and by continued operation to extend the cloud progressively throughout the period of observation. This did not occur, the cloud conserving its crescent shape once formed throughout the twenty minutes of observation, and despite its having traversed a horizontal distance of 30 km. and undergone a change in the direction of its motion after ten minutes. Thus the possibility of the cloud having

developed its shape entirely as a result of wind shear seems remote.

4.3.2 Optical thickness

Optical thickness of a chemical release is the apparent 'flattening' of one side of a spherical cloud which is viewed by resonance radiation. This occurs when the density of the cloud is relatively high, and all solar photons of the appropriate energy are absorbed and re-emitted by cloud atoms on the sunward side. No photons of the appropriate energy remain to penetrate to the other side of the cloud, which is therefore invisible.

This effect is frequently observed in strontium thermite releases, because the high evaporation efficiency of strontium produces a dense cloud. In all such cases the cloud appears 'flattened' from the outset, with a fairly distinct cut-off of visibility as shown in fig. 4.5. In some cases an optically thick cloud subsequently becomes completely visible, because the density decreases as the cloud expands and eventually solar photons of the appropriate energy can reach all regions of the cloud.

In the case of cloud P38H, however, the initial release appeared to be more or less spherical, and similar in shape to other releases which were not optically thick (see fig. 4.6). The 'flattening' of one side of the cloud developed steadily during the first 240 seconds of observation, and then persisted for the rest of the cloud's lifetime. Thus the effect increased with time, rather than decreasing as would be expected if it were caused by optical thickness. In addition, the flattened side of the cloud was approximately its sunward side and not its anti-solar side,

although precise measurements have not been carried out to determine the orientation of the crescent relative to the cloud-sun line.

Thus the behaviour of this cloud is not consistent with its being optically thick.

4.3.3 Differential velocities of superimposed neutral and ionised components

Having concluded that neither wind shear nor optical thickness can account entirely for the shape developed by cloud P38H, an alternative mechanism has been sought to explain this effect.

In view of the possibility that the cloud consisted of superimposed neutral and ionised components, as suggested by the photographs taken through a narrow band filter, the probable behaviour of such a combination in a weak electric field has been investigated. Even if the electric field were not strong enough to cause separation of the two components, it seems likely that some distortion of a spherical cloud would result from the differing forces acting on neutral particles and ions.

4.4 Theory of Gurevich and Tsedilina applied to P38H

It has already been mentioned in section 2.3 that the theory of Gurevich and Tsedilina, which predicts that an ion cloud will tend to split into two regions of maximum density, can be adapted for use in circumstances where there is no separation of ion and neutral clouds in a chemical release experiment (Giles and Martelli, 1971).

Giles and Martelli have derived an expression relating the velocity $\underline{v}_n$ of the neutral particles, and the velocities $\underline{v}_1$ and $\underline{v}_2$ of the field aligned and non field aligned groups

of ions. This expression is

$$\underline{v}_n = \underline{v}_2 + \gamma_i(\underline{v}_1 - \underline{v}_2) \times \underline{e}_B \qquad (4.1)$$

where all symbols are as defined in chapter 2, and working in the magnetic co-ordinate system. In the case of this particular cloud, the above expression can be used to establish whether the shape of the cloud is consistent with the three points chosen for triangulation (the 'top', 'middle' and 'bottom') having the three velocities in the equation.

It is assumed that one end of the cloud has velocity $\underline{v}_n$ and the other end velocity $\underline{v}_1$. Thus by substituting values from table 4.1, a value for $\underline{v}_2$ can be calculated and compared with the measured velocity of the 'middle' of the cloud.

The expressions for the components of $\underline{v}_2$, in terms of $\underline{v}_n$ and $\underline{v}_1$ are

$$v_{2x} = \frac{1}{1+\gamma_i^2}(v_{nx} + \gamma_i v_{ny} + \gamma_i^2 v_{1x} - \gamma_i v_{1y}) \qquad (4.2)$$

$$v_{2y} = \frac{1}{1+\gamma_i^2}(v_{ny} - \gamma_i v_{nx} + \gamma_i^2 v_{1y} + \gamma_i v_{1x})$$

Using the pair of equations 4.2, four sets of values for v_{2x} and v_{2y} have been calculated. These are the values which would apply if

1) the bottom of the cloud has velocity $\underline{v}_n$ and $\gamma_i = 1$
2) the bottom of the cloud has velocity $\underline{v}_n$ and $\gamma_i = 2$
3) the top of the cloud has velocity $\underline{v}_n$ and $\gamma_i = 1$
4) the top of the cloud has velocity $\underline{v}_n$ and $\gamma_i = 2$.

The precise value of γ_i for this experiment is not known, but it is expected to be about 1 or 2, so both these values have been tried.

The values of v_{2x} and v_{2y} obtained in these calculations are shown in table 4.2, together with the measured velocity

components of the 'middle' of the cloud. It will be seen that case 1 above gives the closest agreement between measured and calculated values. Figs. 4.7 and 4.8 show the three velocity vectors $\underline{v}_n$, $\underline{v}_1$ and $\underline{v}_2$, for each of the four cases considered, in the plane perpendicular to the magnetic field lines. As these diagrams show, there is a geometrical relationship between the three vectors, so that the tip of the vector $\underline{v}_2$ must lie on the circumference of a circle whose diameter is the line joining the tips of vectors $\underline{v}_n$ and $\underline{v}_1$.

Thus the crescent shape developed by the cloud is consistent with it containing both neutral particles and ions, and being acted on by a weak electric field. Indeed, in these circumstances, it appears that a crescent shape is an inevitable consequence of the geometrical relationship mentioned above.

4.5 Results obtained by applying theory of Gurevich and Tsedilina to cloud P38H

It has been established, on the basis of the theory of Gurevich and Tsedilina, that the shape developed by cloud P38H is consistent with the top of the cloud moving with velocity $\underline{v}_1$ (the field aligned ion velocity) and the bottom moving with velocity $\underline{v}_n$ (the neutral particle velocity). Thus the measured velocities of different points on the cloud can be used in calculating values for the neutral wind velocity and the electric field. The neutral wind velocity is simply the velocity of the bottom of the cloud, given in table 4.1, i.e. 31ms^{-1} in a direction approximately 30^{o}west of north.

The expression for the electric field perpendicular to the

magnetic field lines is equation 2.8, i.e.

$$\underline{E}_\perp = \underline{B} \times \underline{v}_1 + \xi \underline{B}(\underline{v}_2 - \underline{v}_1) + \eta (\underline{v}_2 - \underline{v}_1) \times \underline{B}$$

but it can be seen from table 2.1 that for altitudes above 120 km $\xi \ll 1$ and $\eta \ll 1$, so the expression reduces to

$$\underline{E}_\perp = \underline{B} \times \underline{v}_1$$

Substituting the velocity (given in table 4.1) of the top of the cloud for $\underline{v}_1$ in this expression, we arrive at a value of 1.7 mV/m for $E_\perp$, the direction of this field being approximately eastward.

These values can be shown, by comparison with results of other barium cloud experiments, to be of the order of magnitude which one might reasonably expect under the conditions which prevailed. The neutral wind value is rather lower than the theoretical quiet time values calculated for experiments SP3 and SP4 (see fig. 5.8), and this is consistent with the lower altitude of P38H. The electric field value is very similar to those measured in the auroral zone during magnetically quiet periods (Stoffregen, 1971).

It must be emphasised that both the results presented here are calculated on the assumption that the cloud points chosen for triangulation are in fact the points having velocities $\underline{v}_n$, $\underline{v}_1$ and $\underline{v}_2$. While it has been established in the previous section that the behaviour of the cloud is consistent with this assumption, it is not intended that these results should be looked on as accurate values of neutral wind velocity and electric field. Rather, the fact that these results have been obtained using an alternative ion cloud theory, and are of the expected order of magnitude, is taken as an indication that the theory of Gurevich and Tsedilina may be used with advantage in analysing certain ion cloud experiments.

	γ_i	v_n	v_1	calculated v_{2x}	calculated v_{2y}
Case 1	1	bottom	top	39	3
Case 2	2	bottom	top	40	-3
Case 3	1	top	bottom	24	-7
Case 4	2	top	bottom	22	-1
Measured velocity of cloud centre				$v_x = 34$	$v_y = 4$

(all values in ms^{-1})

Table 4.2 Comparison of calculated values of v_{2x} and v_{2y} with measured velocity of centre of cloud P38H

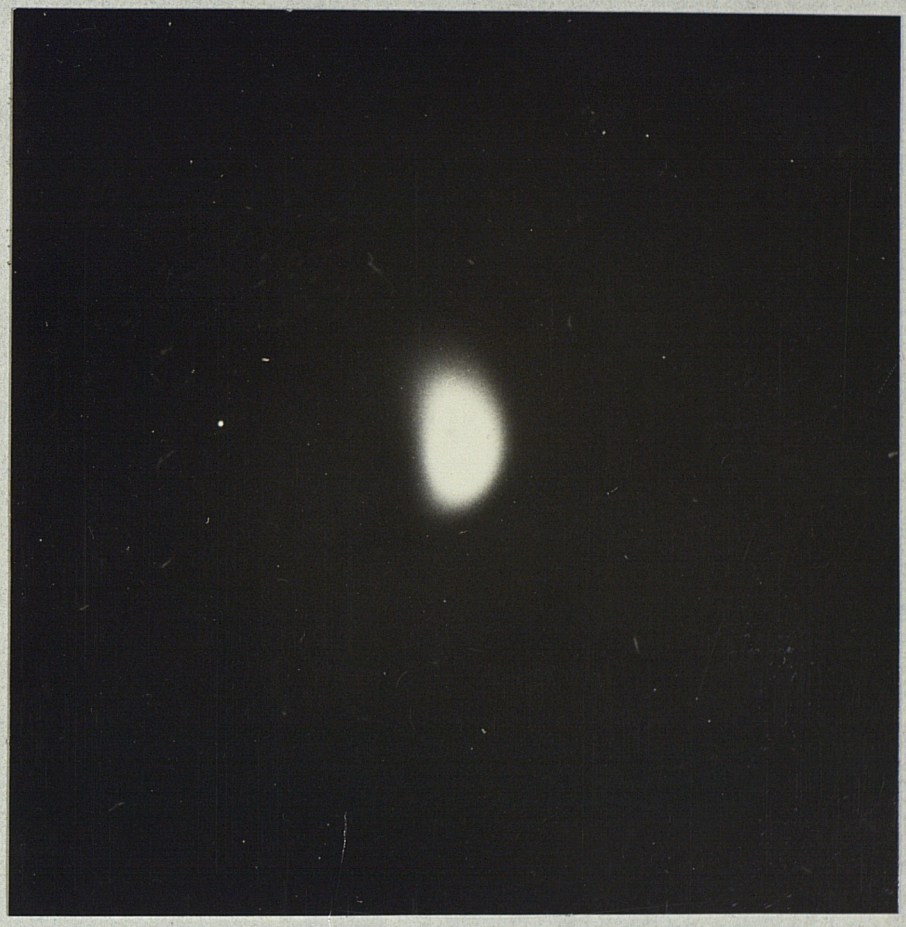

Figure 4.1 Cloud P38H 400 seconds after release, showing crescent shape developed by cloud

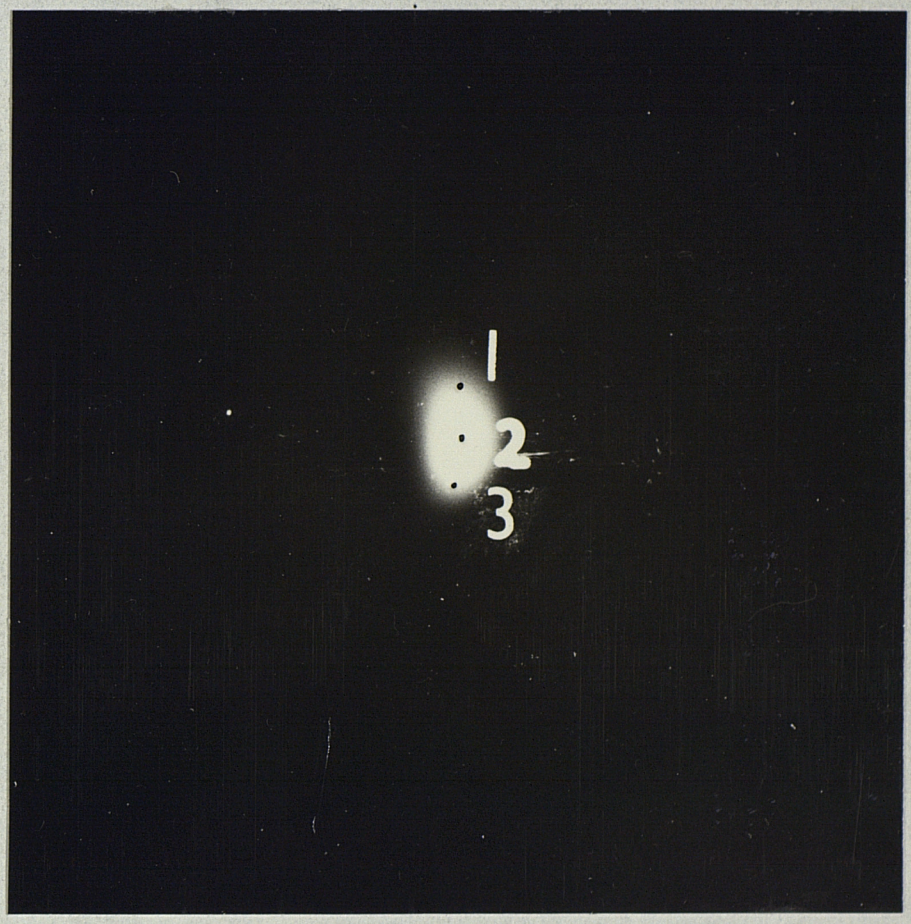

Figure 4.3 Cloud P38H, showing 'top' (1), 'centre' (2) and 'bottom' (3) points used for triangulation

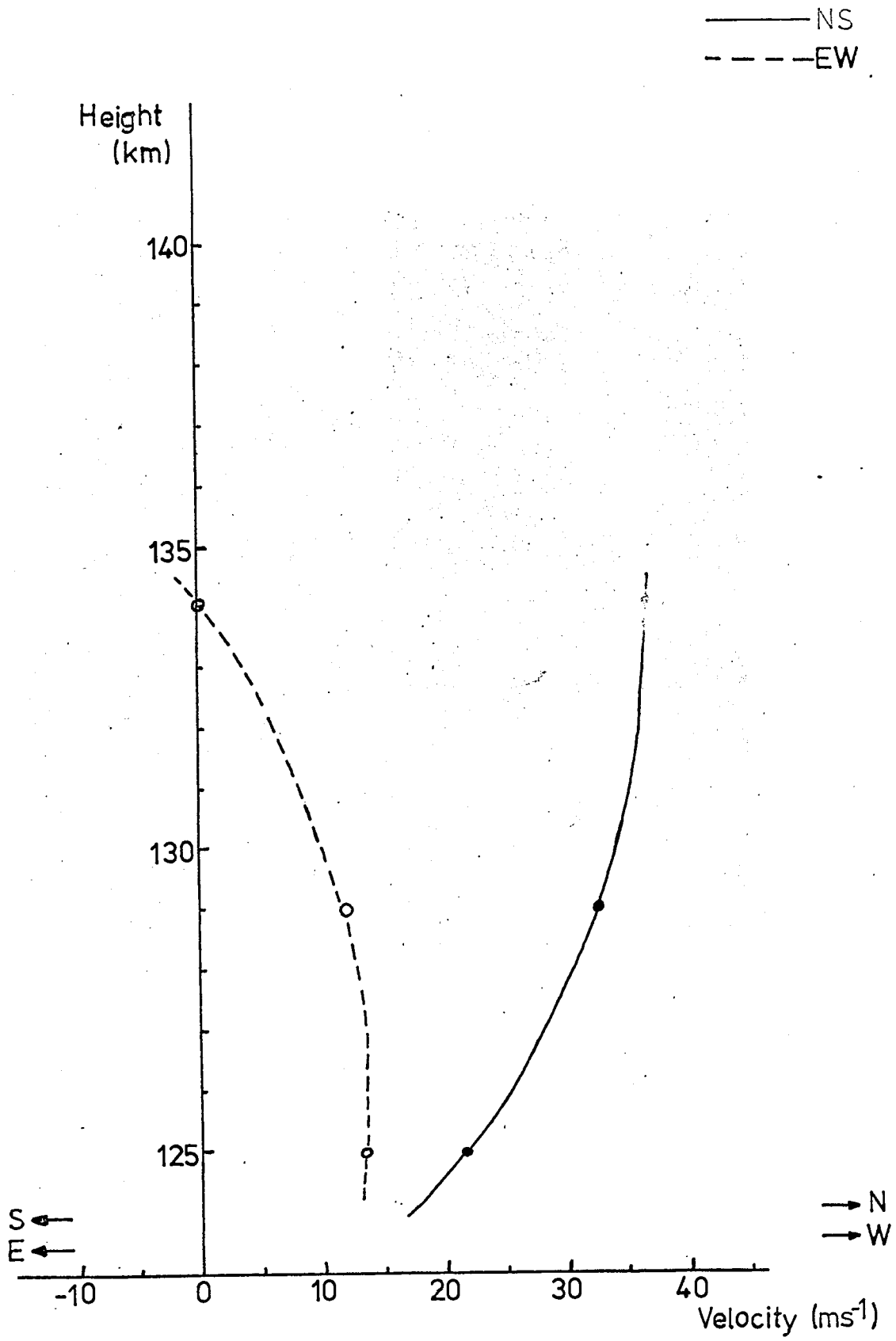

Figure 4.4 N-S and E-W neutral wind components required to produce the crescent shape of cloud P38H by wind shear.

Figure 4.5 Three of the five strontium clouds of experiment K-NA-17, 100 seconds after the first release, showing initial apparent 'flattening' of spherical clouds due to optical thickness

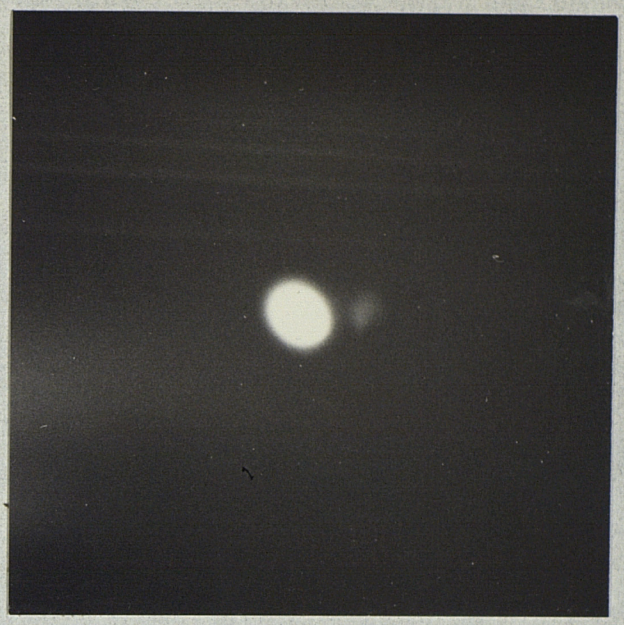

a) Cloud K-NA-16 a few seconds after release. This cloud showed no signs of optical thickness at any stage in its lifetime

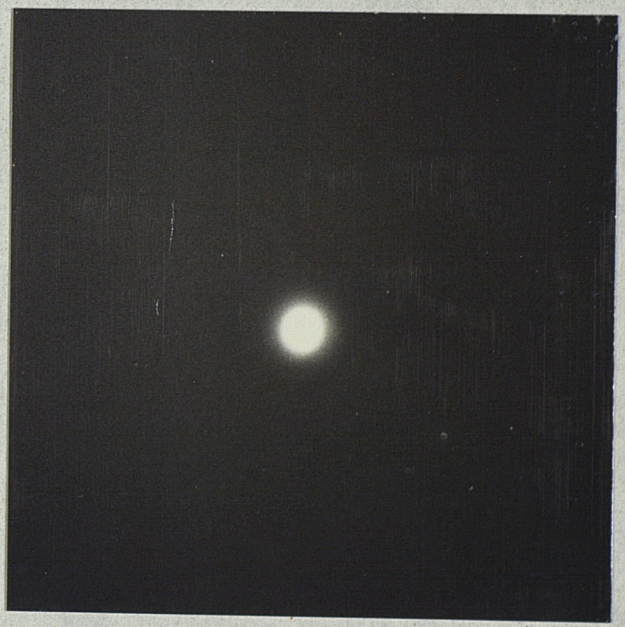

b) Cloud P38H a few seconds after release.

Figure 4.6 Comparison of initial stage of clouds K-NA-16 and P38H, showing similarity in shape, despite later formation of crescent shape in the case of cloud P38H

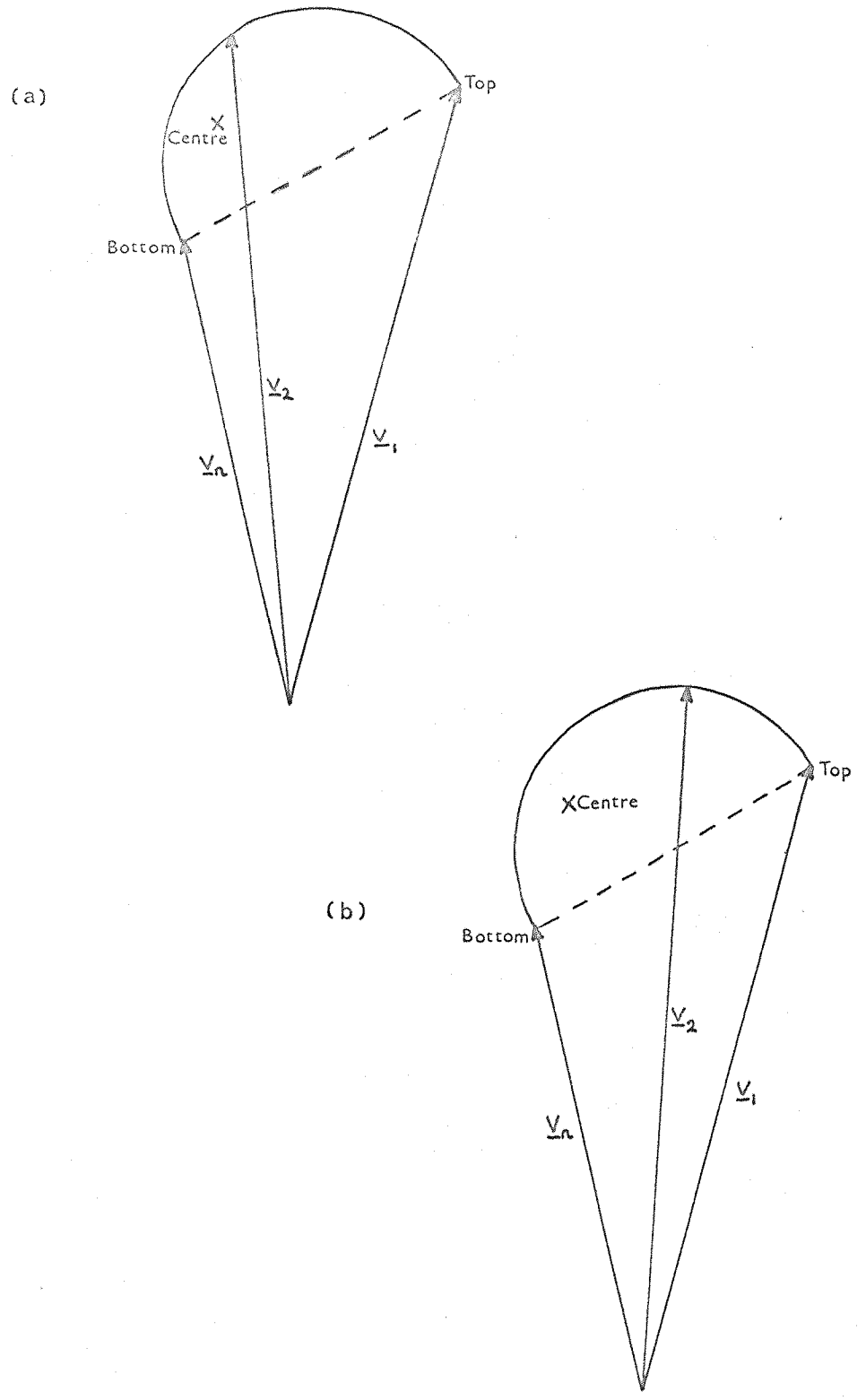

Figure 4.7 Vectors $\underline{V}_n$, $\underline{V}_1$ and $\underline{V}_2$, assuming that the bottom of the cloud corresponds to $\underline{V}_n$ and the top to $\underline{V}_1$. (a) $\gamma_i = 1$, (b) $\gamma_i = 2$

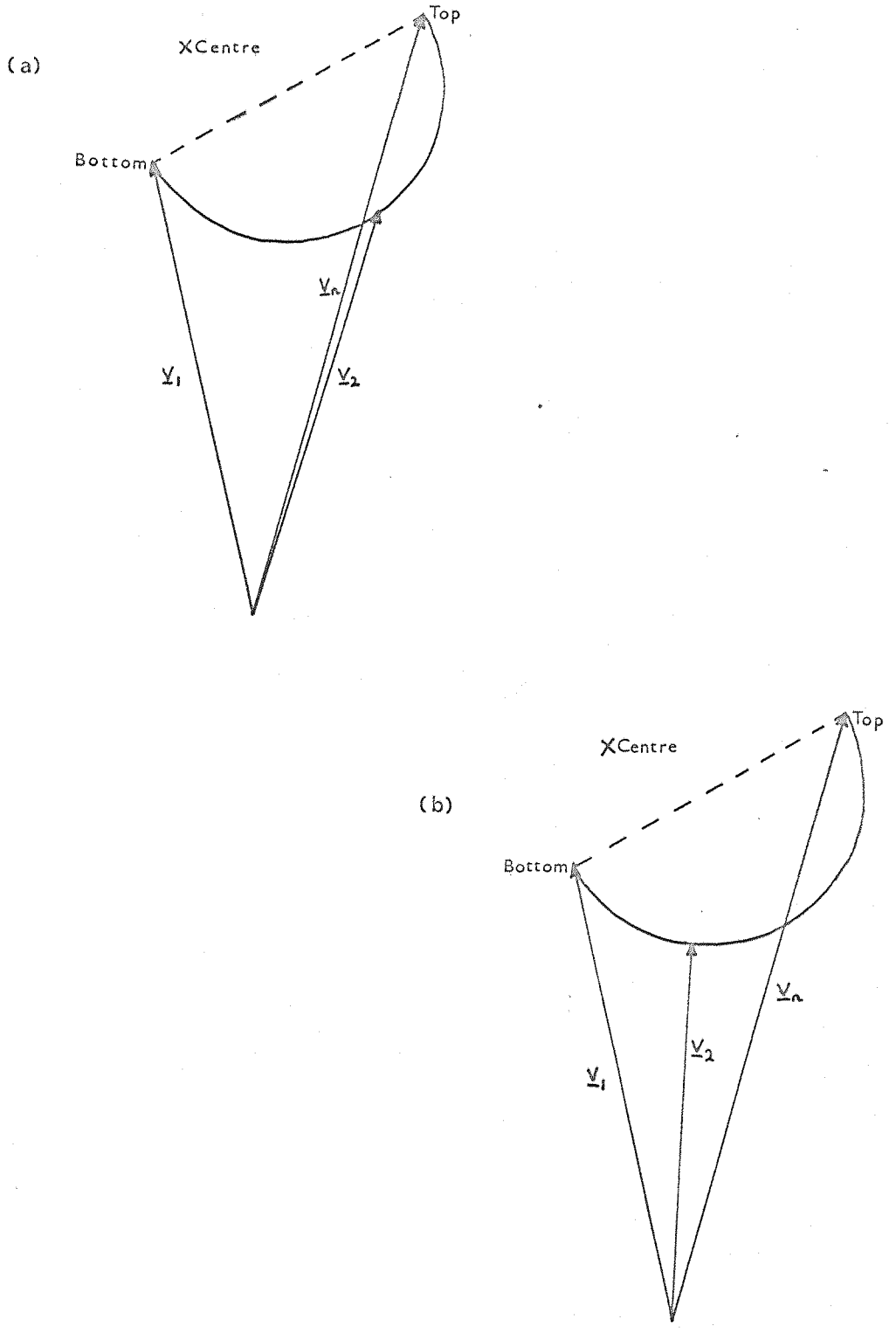

Figure 4.8 Vectors $\underline{V}_n$, $\underline{V}_1$ and $\underline{V}_2$, assuming that the top of the cloud corresponds to $\underline{V}_n$ and the bottom to $\underline{V}_1$. (a) $\gamma_i = 1$, (b) $\gamma_i = 2$

Chapter Five

EXPERIMENTAL EVIDENCE CONCERNING NEUTRAL PARTICLE MOTIONS

5.1 Introduction

A theoretical model for neutral particle motions in magnetically quiet conditions has been described in chapter two. This model gives a horizontal neutral wind vector which undergoes one complete rotation over 24 hours, as shown in figs. 2.5 and 2.6. The wind direction is mainly eastward in the evening and westward in the morning, the reversal occuring at about midnight. Chemical release experiments are usually carried out in twilight conditions. Thus at high latitudes such experiments can be performed throughout the period of this east-west direction reversal by experimenting at different times of year. In magnetically disturbed conditions, the wind system is modified, and by comparing the measured wind vector with the corresponding vector for magnetically quiet times the mechanism producing this modification can be investigated.

Figs. 2.5 and 2.6 show neutral wind vectors for the whole of the northern hemisphere under typical magnetically quiet conditions. For detailed comparison of wind vectors in quiet and disturbed conditions however, a theoretically predicted neutral wind vector pattern, specific to the region and the season in which experiments take place, is required. Such a horizontal wind vector pattern, calculated for Kiruna ($67^{\circ}51'N, 20^{\circ}26'E$) in March 1969, on the basis of the neutral wind model of Kohl and King (1967), is shown in fig 5.1. Vertical neutral wind components are not considered as they are negligible in comparison with the horizontal

components.

During a magnetic substorm a neutral wind system such as that shown in fig. 5.1 may be modified either by additional heating associated with particle precipitation and enhanced Joule effect, or by enhanced ion drag of the neutral atmosphere resulting from increased ion drift velocity, or by a combination of these two effects.

Both of these mechanisms have been investigated theoretically by various authors, and a review article by Rishbeth (1972) discusses the importance on a global scale of various forces in the equations of motion of neutral particles. It has already been mentioned in chapter two that the problem of setting up a theoretical neutral wind model for magnetically quiet times is highly complex and requires several simplifying assumptions to be made. The problems encountered in investigating perturbations to this model are no less complex, and the approximations which must be made in order to obtain a solution mean that such solutions are themselves approximate.

The effect of auroral heating on the neutral atmosphere has been investigated by Cole (1971a,b), who has estimated the relationship between the energy input in the auroral region and the resulting neutral wind velocities in the surrounding region. Rees (1973) has considered the problem of energy transfer from the electric field to the neutral atmosphere. Mayr and Volland (1973) have considered the effect of periodic auroral heating on the composition and motion of the neutral atmosphere. It appears from these theoretical studies that the main energy input from auroral heating occurs in the E-region and results in a convective

motion lifting the neutral atmosphere to F-region heights from where it expands rapidly and radially from the heat source. Burge et al. (1973) have calculated that this effect can produce equatorward winds of up to 50 ms^{-1} in the F-region at low middle latitudes.

Ion drag of the neutral atmosphere has been considered by Fedder and Banks (1972), who investigated the response in time of the neutral atmosphere to a quasi-step electric field of 40 mV/m, simulating the convection electric field during the onset of magnetic disturbance. They find that the magnitude and direction of the neutral wind in the polar cap is controlled by the electric field within one or two hours of its application, the shortest time lag being at low altitudes. They also find that Joule heating associated with the rapid motion of ions through the neutral atmosphere can equal or exceed the influence of solar heating on the neutral particle motions. However, the model set up by Fedder and Banks (1972) excludes global heating effects from the equation of motion of the neutral atmosphere, so that ion drag inevitably appears as the major modifying factor to the quiet time wind system.

It is clear that theoretical models of the neutral atmosphere during magnetic disturbance, are not yet adequate to give information on the relative importance of the various factors (ion drag, Joule heating, particle precipitation) affecting the motion of the neutral particles. Experimental evidence, however, can go some way towards providing this information, and observations of several neutral and ion cloud experiments will now be considered in an attempt to establish which of the above factors most

affects the neutral wind.

5.2 Results of early experiments

The results to be considered initially were obtained from four experiments, carried out on consecutive evenings in Kiruna in March 1969. Details of the experiments are given in table 3.1. The ion drift and neutral wind vectors measured in these experiments are shown in fig. 5.2, together with the theoretical neutral wind vectors associated with the time and height of each release, taken from fig. 5.1. The normal magnetograms recorded at Kiruna throughout the period of these experiments are also shown.

The vectors for experiment K-NA-17, which consisted of five neutral strontium clouds released in magnetically quiet conditions, are shown enlarged in fig. 5.3. It is clear from this diagram that experimental and theoretical neutral wind vectors are in good agreement, both in magnitude and direction, under these conditions.

The neutral wind vectors for barium cloud experiments K-NA-16 and K-NA-18, which were performed during magnetic substorms in the period before breakup, show a marked change in magnitude and direction from the quiet time neutral wind pattern. The observed vectors are considerably enhanced in magnitude compared with their quiet time counterparts, and the directions are south west or west as opposed to the predicted directions of south east or east.

The neutral wind vector for barium cloud experiment P11K, performed in fairly quiet magnetic conditions, shows the same change in direction from predicted south east to observed south west, but a less marked enhancement in magnitude.

In all three barium cloud experiments the ion drift vectors were directed to the south west, the magnitudes of these vectors being related to the degree of magnetic activity in the period immediately preceeding the release.

These observations are consistent with the general pattern for ion drift and neutral wind vectors described by other authors. Stoffregen (1971) has collected and analysed data from eighteen chemical release experiments performed in Kiruna, including the four experiments just mentioned. Most of the experiments reported by Stoffregen were performed in the evening, and showed the ion drift vector directed westward in magnetically disturbed conditions before breakup. The few experiments performed after breakup or in the morning showed a south easterly and an easterly ion drift respectively. The information on neutral winds collected from these experiments shows that observed and theoretical wind vectors are in reasonable agreement in magnetically quiet conditions. During magnetic disturbance the observed wind vector changes from an eastward to a westward direction in the evening, bringing it close to the direction of the ion drift vector.

Wescott et al. (1969) and Meriwether et al. (1973) have reported on neutral wind and ion drift measurements obtained from morning and evening releases in the auroral zone and the polar cap. The observations made from evening releases agree with the auroral zone pattern just described. Morning releases, made simultaneously in the auroral zone and polar cap, showed south westward neutral wind vectors, these vectors being directed towards regions of auroral activity as shown in fig. 5.4. Largely because of this, the authors

reject the possibility of auroral heating as the mechanism for modifying the quiet time neutral wind pattern, since the wind vector should be directed away from the auroral heat source, especially in the polar cap region. Meriwether et al. (1973) conclude that ion drag of neutral particles is the important modifying mechanism to quiet time neutral wind patterns. However, they state that some additional mechanism would be required to explain the morning release results shown in fig. 5.4, since the neutral wind vectors are not directed parallel to the ion drift vectors. They suggest that non parallel neutral wind and ion drift vectors, observed immediately after breakup, can be explained by a time lag between the change in direction of ion motion and the taking up of this change by the neutral particles. To explain the results of morning observations, they suggest that at dawn the ionosphere has not been sunlit for long enough to produce a level of ionisation sufficient for strong coupling of ion and neutral particle motions.

Despite the evidence shown in fig. 5.4, which appears contrary to what would be expected if auroral heating were the mechanism modifying the quiet time neutral wind pattern, it is possible to explain these observations in terms of auroral heating, if the entire auroral zone is considered. Fig. 5.5 shows the position of Scandinavia relative to the auroral zone at different times of day, and thus shows the typical auroral forms which are observed during the night. From this it can be seen that, while some auroral forms may be seen in the early evening or early morning, the main auroral activity occurs a little before local midnight, and so the auroral heat source is in the region which has this

local time. Modified neutral winds, directed radially from this heat source could thus blow towards weaker auroral forms in the region of chemical release experiments. This possibility is supported by pictures of aurora obtained from the U.S.A.F. 'DAPP' satellite. These have shown that the region of auroral activity can be very large, extending well into the polar cap during the later phases of a substorm. Pictures taken at times similar to the release times of the apparently anomalous experiments reported by Meriwether et al. (1973), show extensive auroral activity well to the north of the release area in addition to weaker auroral arcs in or near this area.

Thus the neutral winds observed in these experiments can be explained in terms of either ion drag or auroral heating as the major factor affecting the quiet time wind system. However, certain assumptions made in applying these explanations can be tested by performing further experiments under specific conditions. Meriwether et al. (1973) assumed that a time lag following breakup and insufficient ionisation at dawn would inhibit the operation of ion drag. This can be tested by releases made under the following conditions:

1) during magnetic disturbance, so that the modifying mechanism will be operative.
2) at a time when the ionosphere has been sunlit for several hours, so that a high level of ionisation is maintained.
3) near or after local midnight, so that the neutral atmosphere has had ample time to follow the west to east direction change undergone by the ion drift

vector at breakup.

These conditions can be realised in practice by making releases at high latitude in late spring or late summer. Experiments cannot be performed nearer to the summer solstice, because of the normal requirement in chemical release experiments for a reasonably dark sky background. From fig. 5.6, showing sunrise and sunset at the latitude of Kiruna, it can be seen for example that conditions here fulfil our requirements in mid April or late August.

5.3 Results of further experiments

Two sets of experiments have been carried out under conditions as near as possible to those set out at the end of the previous section. Two barium cloud releases were made from Kiruna in late April 1971, at times just after local midnight. Data was also obtained from two barium cloud releases made from South Uist in mid May 1973 at times shortly before local midnight. Details of these four releases are given in table 3.1.

5.3.1 The Kiruna experiments

The first of these two releases was made after several hours of considerable magnetic activity and well into the negative phase of the substorm. At the release height of 170 km., the ionosphere is permanently sunlit at the end of April, and so all three conditions described in section 5.2 were met for this experiment. The observed neutral wind and ion drift vectors for experiment P63K are shown in fig. 5.7, together with the theoretical neutral wind vector and the Kiruna normal magnetograms for several hours on either side of the release time. From this diagram it can be seen that the neutral wind direction was close to the predicted quiet

time direction, but that its magnitude was considerably enhanced by the magnetic activity. The ion drift vector pointed to the south east, in a direction making an angle of 100° with the neutral wind vector.

The second experiment was performed, for comparison, in a period of magnetic quiet, and the results are also shown in fig. 5.7. The directions of all vectors were similar to those for experiment P63K, but in the magnetically quiet conditions, the magnitudes of the neutral wind and ion drift vectors were smaller than in the first experiment (in the case of the ion drift, very much smaller).

The results of experiment P63K are not consistent with ion drag being the major factor modifying the quiet time wind system. In this experiment, the direction of the observed neutral wind was rotated slightly to the west of the predicted direction, whereas the ion drift vector was directed about 90° to the east of this theoretical vector. Thus there is no evidence that the neutral particles were following the direction taken by the ions, and no apparent reason why the ion drag effect should not be observed if it were indeed the modifying mechanism for the quiet time wind system.

Rather, the results obtained are consistent with a wind system modified by additional auroral heating. The principal source of this heating would appear to be situated to the north east of the release point in the case of both experiment P63K and experiment P54K. In the former experiment, the high degree of magnetic activity would be associated with considerable additional heating and enhancement of the magnitude of the neutral wind, but in

the latter case, the magnetically quiet conditions would correspond to a very weak heat source and so the observed neutral wind vector would be of similar magnitude to the theoretical quiet time vector. It can be seen from fig. 5.7 that the observations are in reasonable agreement with this behaviour pattern.

5.3.2 The South Uist experiments

Conditions in South Uist in mid May are somewhat similar to those existing in Kiruna at the end of April. The ionosphere above 200 km. is permanently sunlit at this time, and between 150 and 200 km. it is sunlit for at least twenty hours each day. South Uist is about 10^{o} latitude to the south of the auroral zone and electric fields are expected to be weaker here than in the auroral zone. Therefore ion drag would be less effective in modifying the quiet time neutral wind system. However, the effects of additional auroral heating are dependent on conditions at the heat source rather than on local conditions at the release point, and so would be little affected by the change of latitude.

The two releases were made on consecutive nights, in magnetically disturbed conditions. The first release was made during the negative phase of a substorm, and the second just before the onset of a negative bay. The neutral wind and ion drift vectors observed in these experiments are shown in fig. 5.8, together with corresponding theoretical neutral wind vectors (calculated for this purpose on the basis of the model of Kohl and King (1967)), and the magnetogram showing the H component of the geomagnetic field at South Uist.

In experiment SP3, no separation of neutral and ionised

components was observed. The neutral wind was enhanced by a factor of four in magnitude over its quiet time value, and was directed to the south west instead of the predicted south easterly direction.

The results of the second experiment show a similar direction for the observed neutral wind, but the magnitude is enhanced only by a factor of two in this case. An ion cloud was observed in this experiment, and the ion drift vector pointed to the south east, making an angle of about 90° with the neutral wind vector. The magnitude of the ion drift vector was about half that of the observed neutral wind vector.

Again, the rsults of the experiments do not support the ion drag theory. In the first experiment the ion drift vector was so small that no separate ion cloud was observed, but the neutral wind was greatly enhanced. In the second experiment the ion drift vector was larger than in the first, but the enhancement of the neutral wind was smaller.

The results are instead consistent with the auroral heating theory, where the magnitude of the enhanced neutral wind would depend on the degree and duration of magnetic activity in the period before the release. The south westerly direction of the observed neutral winds in the two experiments are consistent with a heat source in the auroral zone (to the north of the release area) and at or near local midnight (to the east of the release area).

5.4 Conclusions

From the experiments described in the two previous sections the following picture of neutral wind and ion drift velocities emerges.

1) At magnetically quiet times, the neutral wind in auroral and sub-auroral regions is similar to the theoretically predicted wind, based on Jacchia's exospheric temperature distribution. In general, the ion drift velocities are smaller than the neutral wind velocities.

2) At magnetically disturbed times the neutral wind velocities are of much greater magnitude than at quiet times (enhanced by up to a factor of ten). The ion drift velocities are also large, but the magnitudes of the two velocities do not appear to be directly related. The directions of motion of the neutral particles and the ions are time dependent in the following manner.

   a) In the evening before breakup, ions drift to the west and neutral particles move in roughly the same direction.

   b) In the evening after breakup, ions drift to the east but neutral particles continue to move westward.

   c) In the morning, the ion drift is to the south east and neutral particles move to the south or south west.

This picture of neutral winds during magnetic disturbance would appear to point to auroral heating being the dominant mechanism for modifying the quiet time wind system. This auroral heating is caused by both enhanced particle precipitation and Joule effects and the principal heat source appears to be located in the post-breakup recovery region; i.e. at or shortly after local midnight.

The failure of neutral particles to follow the direction of ion drift after breakup (even on the time scale

calculated by Fedder and Banks (1972)) and in the morning (even when the ionosphere is permanently sunlit) suggests that ion drag is less important than auroral heating in modifying neutral particle motion.

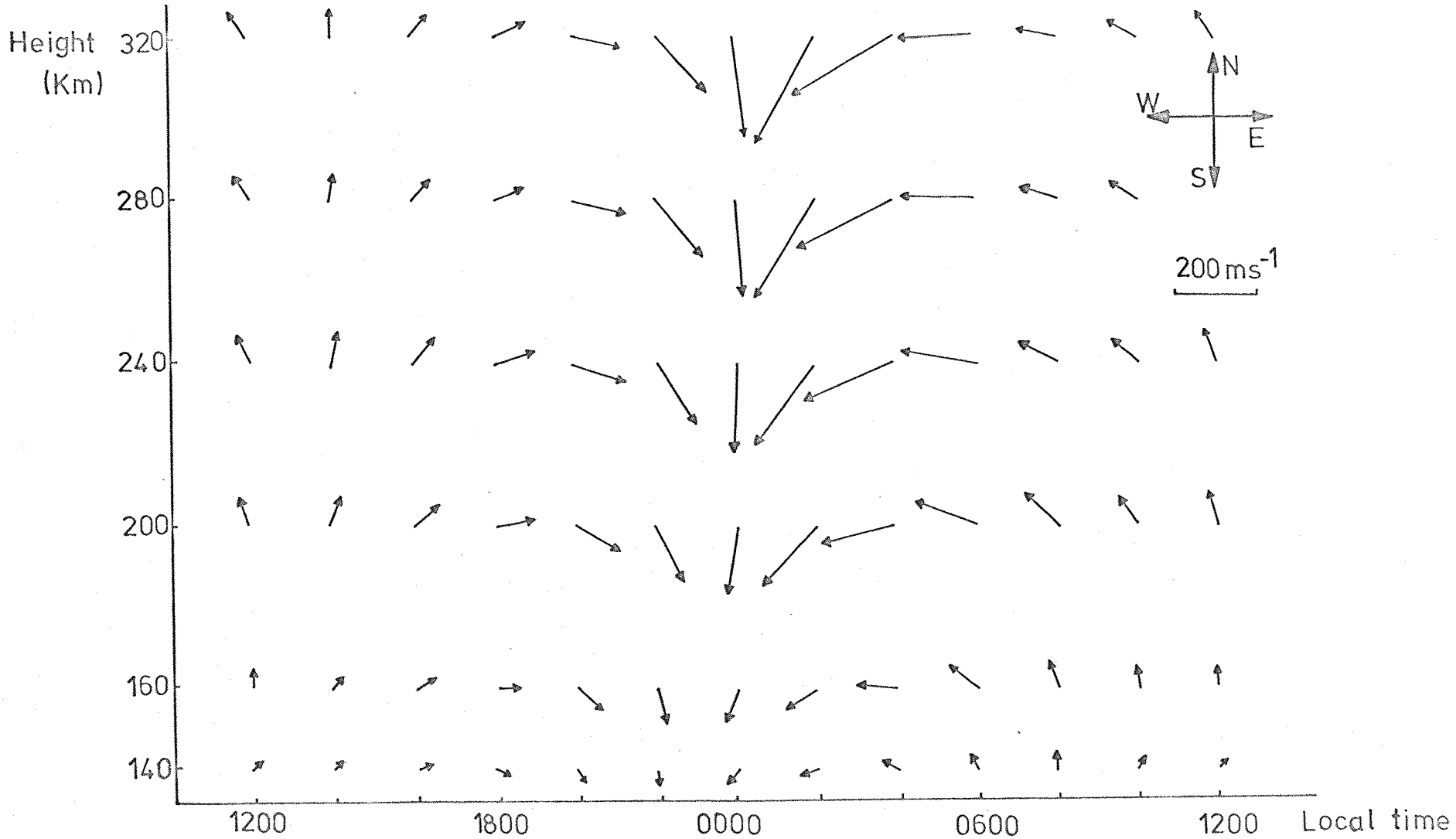

Figure 5.1 Example of the neutral wind system computed for magnetically quiet times (Kiruna, March 1969)
The information shown in this diagram has been made available by the courtesy of Dr.J.King

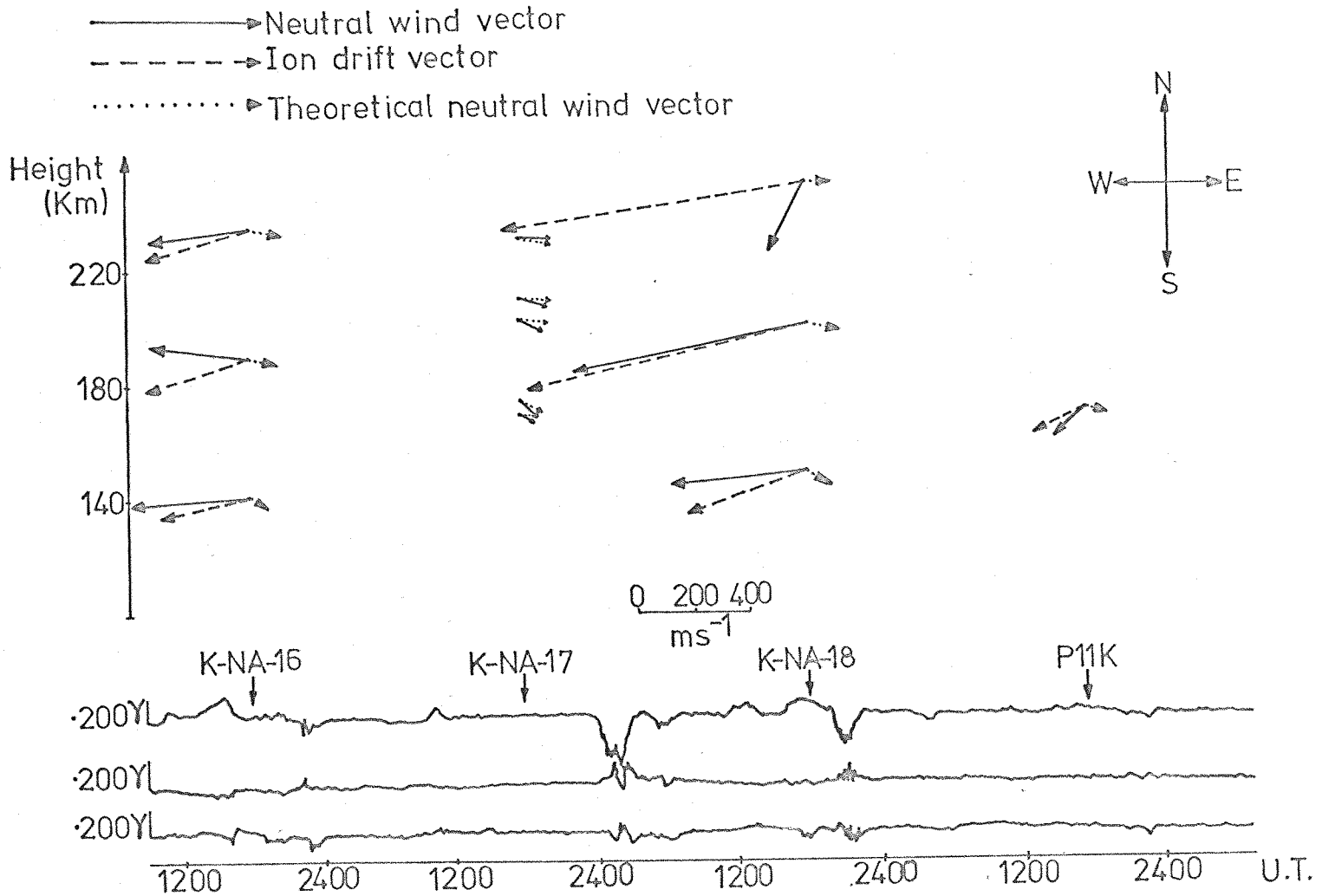

Figure 5.2 Observed ion cloud drift and neutral wind velocities in four release experiments from ESRANGE, Kiruna, in March 1969. The computed quiet time wind vectors are also shown.

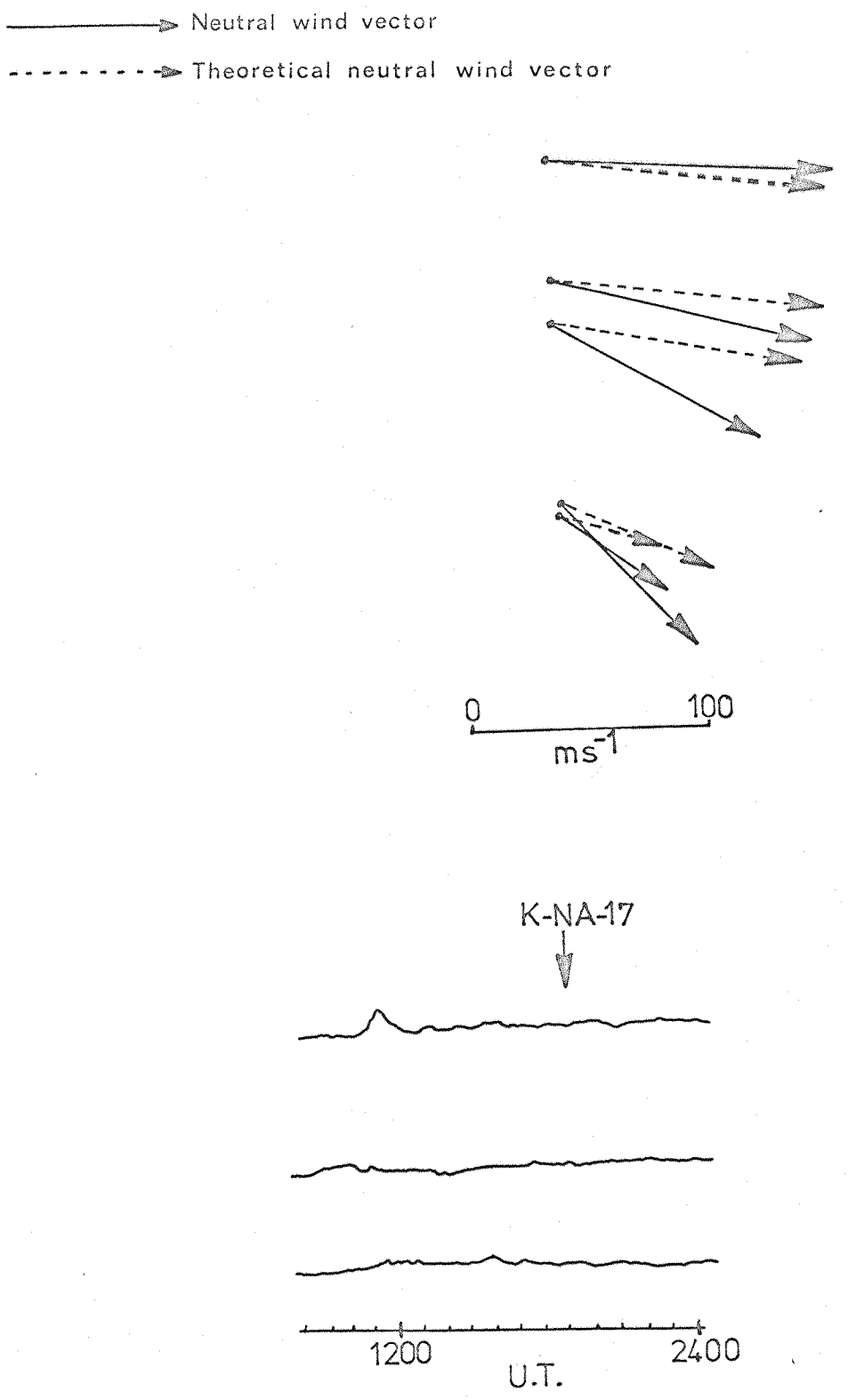

Figure 5.3 Enlarged detail of the five strontium releases on 16th March 1969, comparing the observed and computed quiet time wind velocities.

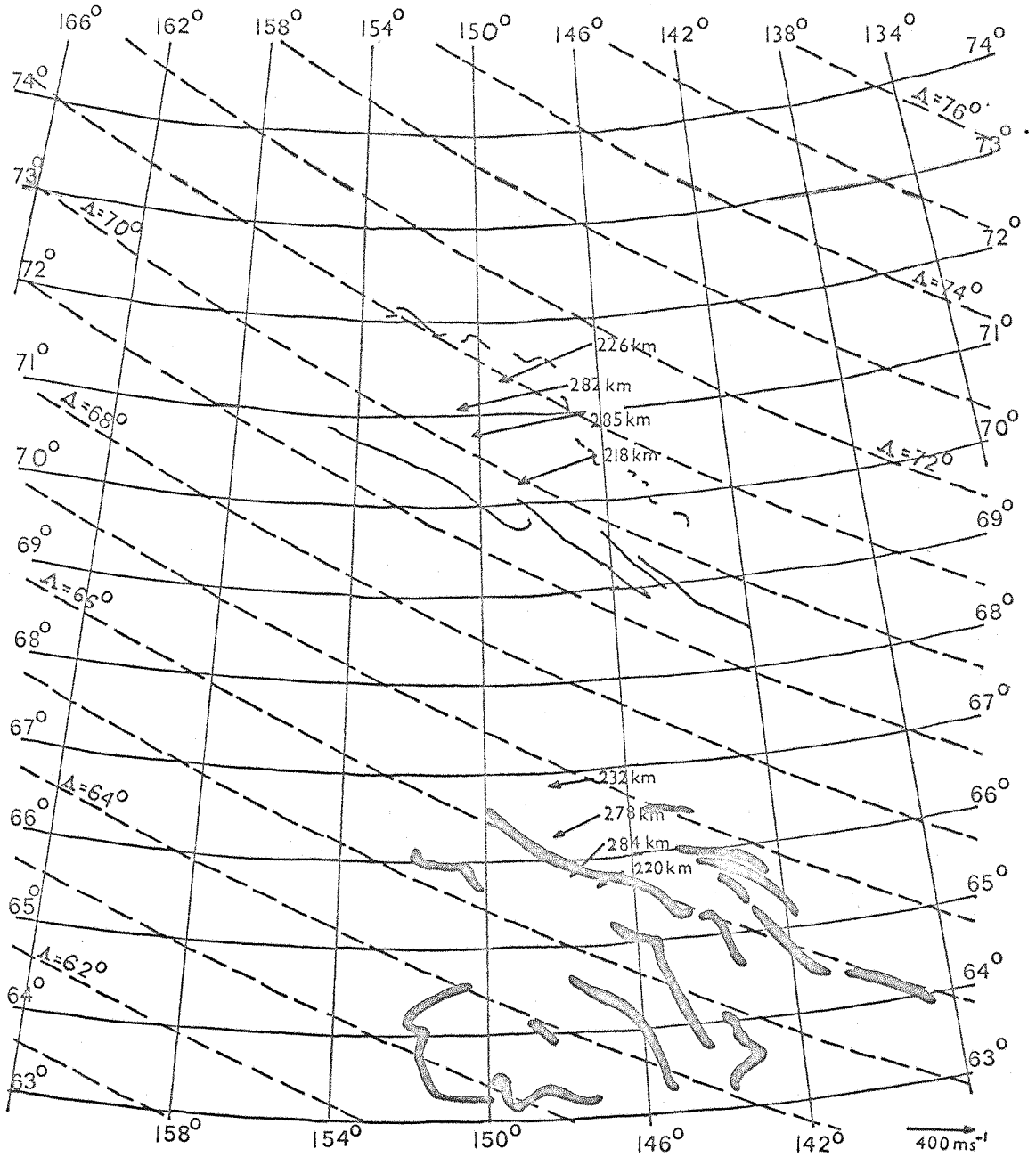

Figure 5.4 Neutral wind vectors and location of auroral forms for morning releases in the polar cap and auroral zone in March 1970. (After Meriwether et al., 1973.)

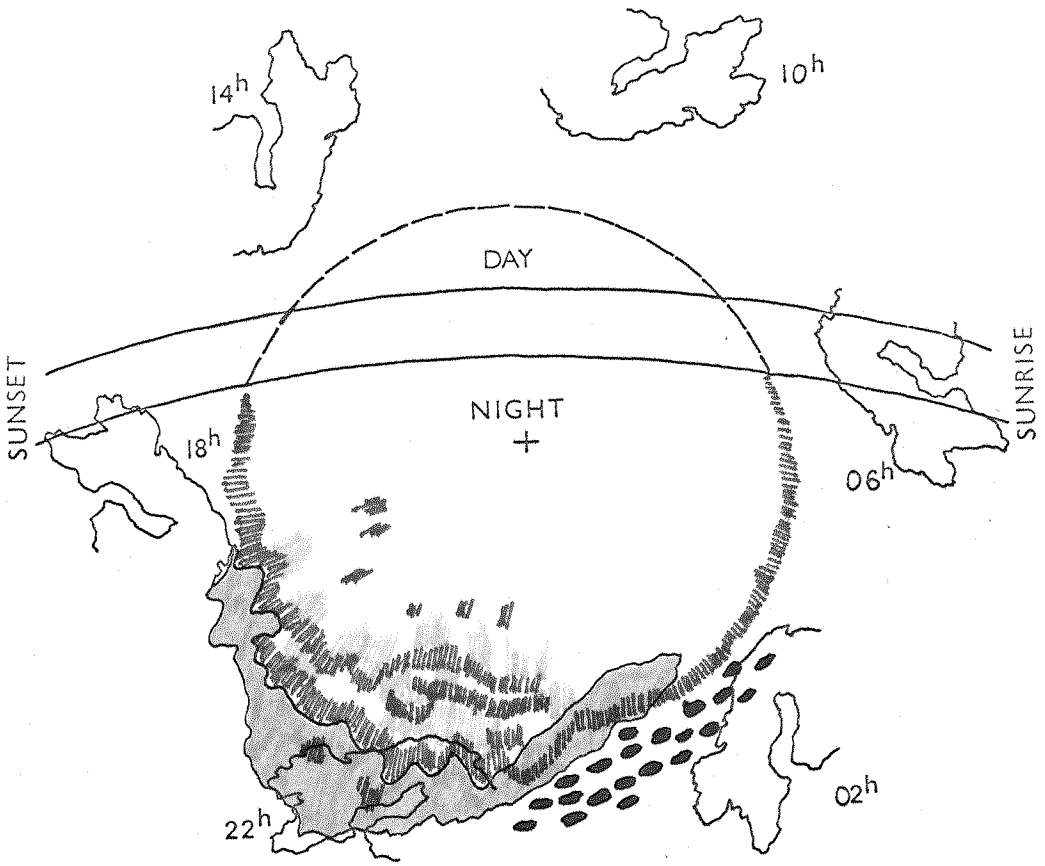

Figure 5.5 The position of Scandinavia with respect to the auroral zone during one day (after Stoffregen, 1971).

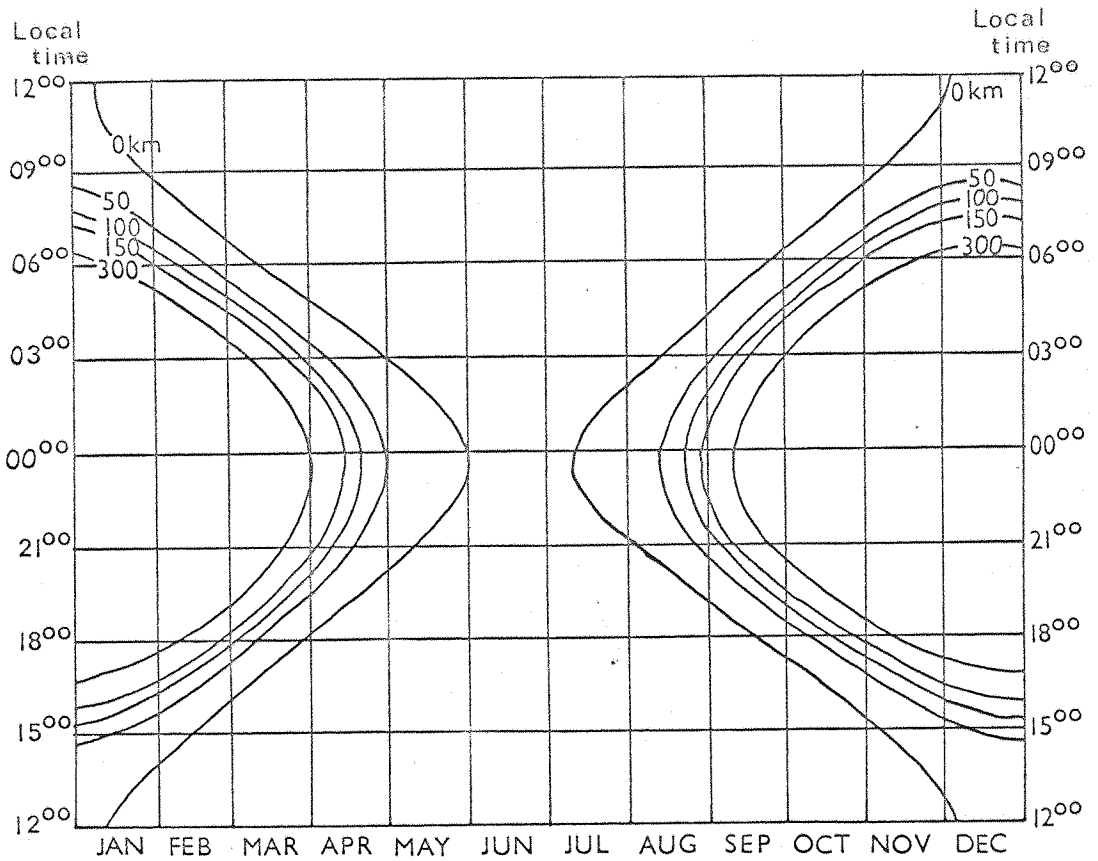

Figure 5.6 Height of the earth's shadow for different seasons and heights at the latitude of Kiruna (after Stoffregen, 1971).

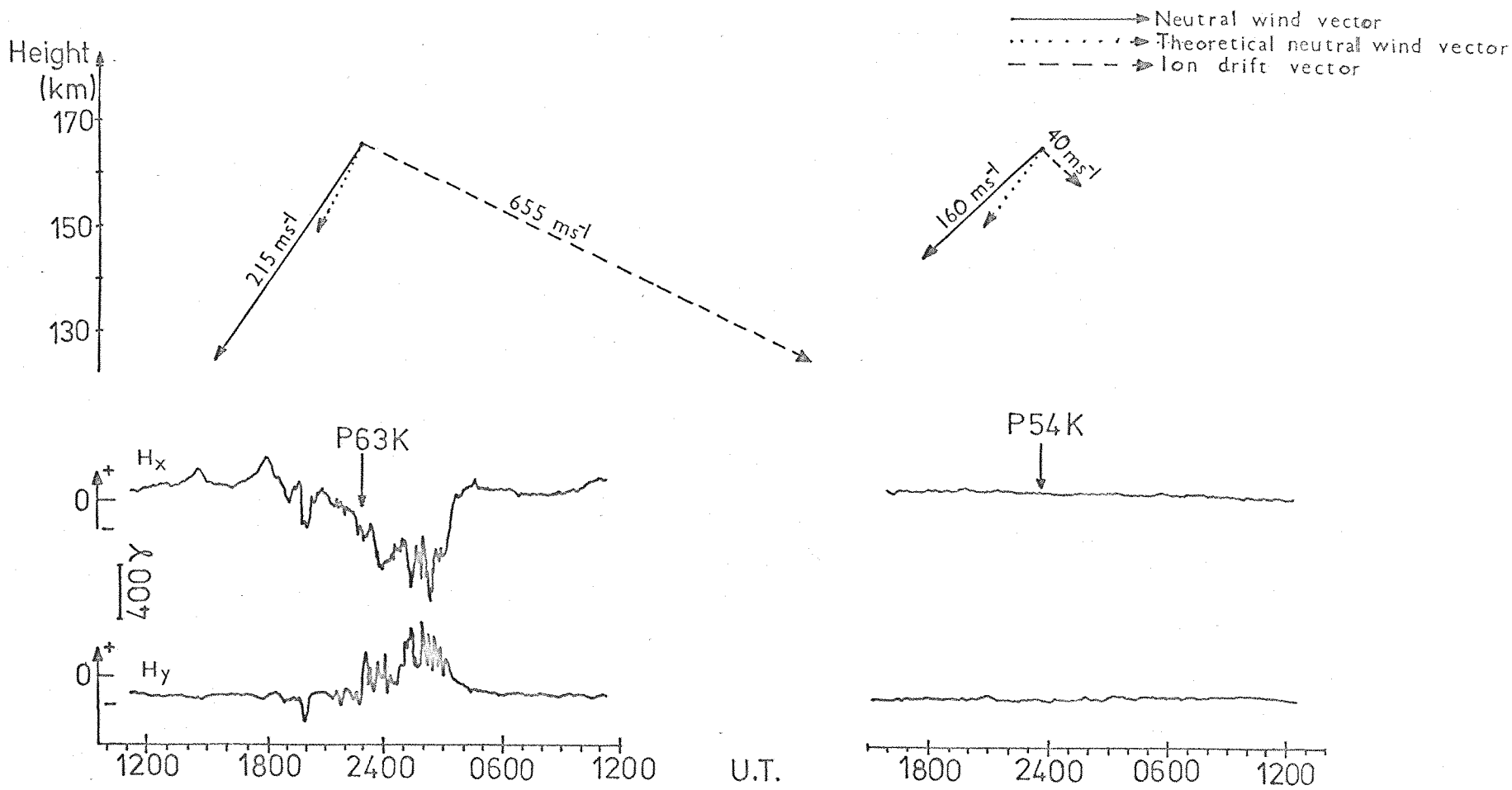

Figure 5.7 Observed ion cloud drifts and neutral wind velocities from two releases in Kiruna, on 21 and 24 April 1971. The computed quiet time neutral wind vectors are also shown.

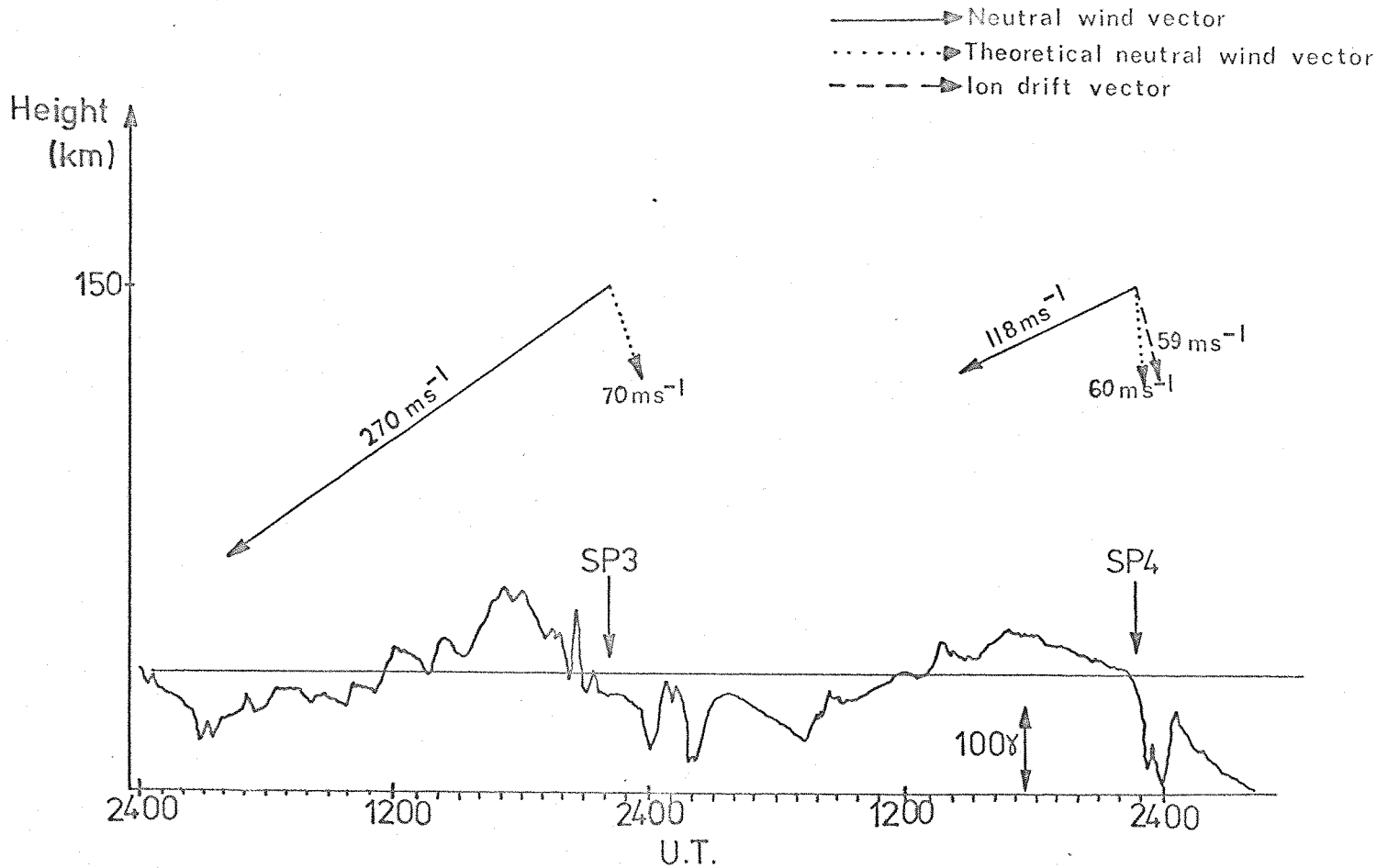

Figure 5.8 Observed ion cloud drift and neutral wind velocities from two releases in South Uist, in May 1973. No separation of ionised and neutral components was observed in the release made on 15 May. The computed quiet time vectors are also shown.

Chapter Six

SUMMARY

6.1 Ionospheric electric fields

Measurement of ionospheric electric fields, using barium ion clouds, is now a well established technique. Many such measurements have been made at altitudes around or above 200 km, and both the electric field patterns in these regions and their relation to magnetic disturbance have been reported by Heppner (1972). However, lower altitudes , particularly those below 150 km, have largely been ignored because of altitude restrictions imposed by the Haerendel theory used for ion cloud analysis.

It has been shown in chapter four that barium clouds at E-region altitudes can be analysed using an alternative theory, derived by Giles and Martelli (1971) on the basis of a more general consideration of plasma inhomogeneities by Gurevich and Tsedilina (1967). A special case of this theory has been applied to a cloud which did not separate into neutral and ionised components but may have contained ions, demonstrating that this theory can be applied in circumstances where the Haerendel theory cannot be used. Thus it seems likely that further information concerning ionospheric electric fields could be obtained using this alternative theory, both at lower altitudes than have normally been considered, and when electric fields are small and separation may not occur.

6.2 Ionospheric neutral winds

The predictions of a neutral wind theory of Kohl and King (1967) for magnetically quiet times, are supported by the results of quiet time neutral cloud releases described in

chapter five.

The problem of the relative importance of two mechanisms which are likely to modify this neutral wind system during magnetic disturbance has also been considered. The two mechanisms: enhanced ion drag and enhanced auroral heating (due to particle precipitation and/or Joule heating), appear to provide equally acceptable explanations of the observations of evening releases in the positive phase of magnetic substorms. Experiments carried out in the morning, and in the evening during the negative phase of substorms, however, suggest that enhanced auroral heating is the dominant mechanism, with the principal heat source located in the auroral zone or polar cap, and at or near local midnight.

It is thought likely that seemingly anomalous results, where neutral winds were directed towards regions of observable auroral activity, can be explained in terms of enhanced auroral heating if the auroral activity over the entire auroral zone and polar cap regions is taken into consideration.

It would be desirable for further experiments to be carried out in the morning or around local midnight, to give additional information on the probable location of the principal heat source, and possibly to compare this information with large scale photographs of auroral activity taken from polar orbiting satellites.

REFERENCES

Aggson,T.L. (1969) 'Atmospheric Emissions' (edited by B.M.McCormac and A.Omholt) p.305, Van Nostrand Reinhold, New York.

Axford,W.I. and Hines,C.O. (1961) Can. J. Phys. 39, 1433.

Burge,J.D., Eccles,D., King,J.W. and Rüster,R. (1973) J. Atmos. Terr. Phys. 35, 617.

Cole,K.D.(1971a) Planet. Space Sci. 19, 59.

Cole,K.D.(1971b) Planet. Space Sci. 19, 1010.

Fedder,J.A. and Banks,P.M. (1972) J. Geophys. Res. 77, 2328.

Föppl,H.,Haerendel,G., Haser,L., Loidl,J., Lütjens,P., Lüst,R., Melzner,F., Meyer,B., Neuss,H., and Rieger,E. (1967) Planet. Space Sci. 15, 357.

Geisler,J.E. (1966) J. Atmos. Terr. Phys. 28, 703.

Giles,M. and Martelli,G. (1971) Planet. Space Sci. 19, 1.

Groves,G.V. (1960) Nature (London) 187, 1001.

Groves,G.V. and Owen,G. (1960) Photogram. Record 3, 338.

Groves,G.V., Owen,G. and Thorpe,M. (1960) Photogram. Record 3, 370.

Gurevich,A.V. and Tsedilina,E.E. (1967) Sov. Phys. Uspekhi 10, 214.

Haerendel,G., Lüst,R. and Rieger,E. (1967) Planet. Space Sci. 15, 1.

Haerendel,G., Lüst,R., Rieger,E. and Völk,H. (1969) 'Atmospheric Emissions' (edited by B.M.McCormac and A.Omholt) p.293, Van Nostrand Reinhold, New York.

Haser,L. (1967) 'Aurora and Airglow' (edited by B.M.McCormac) p.391, Reinhold, New York.

Heppner,J.P. (1972) J. Geophys. Res. 77, 4877.

Hilmi,H. (1974) M.Phil. thesis, Sussex University.

Hines,C.O. (1965) Planet. Space. Sci. 13, 169.

Hunter,J.R.W. (1970) Ph.D. thesis, Sussex University.

Jacchia,L.G. (1965)'Space Research V'(edited by D.G.King-Hele, P.Muller and G.Righini) p.1152, North-Holland, Amsterdam.

Kaiser,T.R. (1968) Proc. I. A. U. Symp. Phys. and Dynam. of Meteors (edited by Kresak and Millman) p.161, Reidel, Holland.

Kaiser,T.R., Pickering,N. and Watkins,N. (1969) Planet. Space Sci. 17, 519.

King,G.A.M. (1964) J. Atmos. Sci. 21, 231.

King-Hele,D.G. (1964) Planet. Space Sci. 12, 835.

Kochanski,A. (1964) J. Geophys. Res. 69, 3651.

Kohl,H. and King,J.W. (1967) J. Atmos. Terr. Phys. 29, 1045.

Manring,E., Bedinger,J.F., Pettit,H.B. and Moore,C.B. (1959) J. Geophys. Res. 64, 587.

Manring,E., Bedinger,J.F., Knaflich,H. and Layzer,D. (1964) NASA Contractor Report CR-36.

Maynard,N.C. and Heppner,J.P. (1970) 'Particles and Fields in the Magnetosphere' (edited by B.M.McCormac) p.247, Reidel, Holland.

Maynard,N.C. and Johnstone,A.D. (1974) J. Geophys. Res. 79, 3111.

Mayr,H.G. and Volland,H. (1973) J. Geophys. Res. 78, 2251.

Meriwether,J.W., Heppner,J.P., Stolarik,J.D. and Wescott,E.M. (1973) J. Geophys. Res. 78, 6643.

Mozer,F.S. and Bruston,P. (1967) J. Geophys. Res. 72, 1109.

Murphy,C., Bull,G.V. and Edwards,H.D. (1966) J. Geophys. Res. 71, 4535.

Rees,D. (1971) J. Brit. Interplanet. Soc. 24, 233.

Rees,M.H. (1973) Invited paper, IAGA Kyoto Conference, September 1973. (Unpublished)

Rishbeth,H. (1972) J. Atmos. Terr. Phys. 34, 1.

Rosenberg,N.W., Golomb,D. and Allen Jr.,E.F. (1964) J. Geophys. Res. 69, 1451.

Rüster,R. and Dudeney,J.R. (1972) J. Atmos. Terr. Phys. 34, 1075.

Stoffregen,W. (1971) Rept. No.17, Part B. Uppsala Jonosfärobservatorium.

Storey,L.R.O. (1968) 'Earth's Particles and Fields' (edited by B.M.McCormac) p.235, Reinhold, New York.

Taylor,H.E. and Hones,E.W. (1965) J. Geophys. Res. 70, 3605.

Wescott,E., Stolarik,J.D. and Heppner,J.P. (1969) J.Geophys. Res. 74, 3469.